Copy 5
RM E51I07

NACA RM E51I07

RESEARCH MEMORANDUM

EFFECTS OF INTERNAL CONFIGURATION ON AFTERBURNER SHELL TEMPERATURES

By E. William Conrad and Emmert T. Jansen

Lewis Flight Propulsion Laboratory
Cleveland, Ohio

NATIONAL ADVISORY COMMITTEE
FOR AERONAUTICS

WASHINGTON

January 8, 1952

NATIONAL ADVISORY COMMITTEE FOR AERONAUTICS

RESEARCH MEMORANDUM

EFFECTS OF INTERNAL CONFIGURATION ON AFTERBURNER SHELL TEMPERATURES

By E. William Conrad and Emmert T. Jansen

SUMMARY

A brief investigation was conducted in the altitude wind tunnel to determine the extent to which the afterburner shell cooling problem could be alleviated by internal configuration changes. Data were obtained with and without a cooling liner installed and for variations in the radial fuel distribution and in the radial distribution in flame-seat area. Consideration is given to the effects on both shell temperature and afterburner performance.

In the range of fuel-air ratio investigated, the use of a cooling liner resulted in substantial reductions in shell temperature with no penalty in performance. Appreciable reductions in afterburner shell temperature were made possible by control of the radial fuel distribution; however, the effects on performance are uncertain and may depend on other variables not investigated. No direct relation was found between shell temperature and the clearance between the flame holder and the shell; however, some cooling effect may possibly be achieved by trail-and-error procedure.

INTRODUCTION

The performance and operational characteristics obtained during many recent afterburner investigations (see, for example, references 1 to 3) have demonstrated the practicability of this method of thrust augmentation and warrant additional effort toward the solution of installation problems. One of the most important of these problems is obtaining sufficient afterburner cooling to ensure adequate service life with the minimum penalty to aircraft performance. External cooling by means of a secondary air flow is generally used, and the effects of many of the design variables involved have been considered in the analysis of reference 4. The results of a brief investigation made to determine whether afterburner shell temperatures can be appreciably reduced by changes in the internal configuration of the burner without penalizing its over-all performance are given herein.

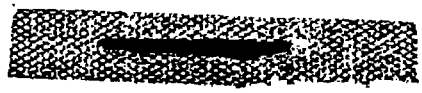

Data are presented to show the effects of changes in the radial distribution of afterburner fuel and of the flame-seat area. In addition, the effects of installing a cooling liner are shown. For each series of configurations, the effect of changing a single variable is considered in terms of (a) the effect on shell temperature and (b) the variation of afterburner performance.

The investigation was conducted in the NACA Lewis altitude wind tunnel using a turbojet engine complete with afterburner and variable-area exhaust nozzle. Data were obtained at limiting turbine-outlet temperature over a range of tail-pipe fuel-air ratio and results are given for operation at altitudes from 15,000 to 45,000 feet at a flight Mach number of 0.19.

APPARATUS AND INSTRUMENTATION

Engine

A typical full-scale axial-flow turbojet engine was used with the afterburner for this investigation. During afterburner operation, the variable-area exhaust nozzle was actuated by the engine control to maintain limiting turbine-outlet temperature over the full range of tail-pipe fuel-air ratios.

Afterburner

Schematic views of the afterburner configurations are given in figure 1 to show the location of the components. The same diffuser outer shell, combustion chamber, and exhaust nozzle were used for all configurations. The diffuser inner cone had a double curved surface for configurations A-1, A-2, and A-3, and a straight conical surface for configurations B-1, B-2, B-3, C-1, C-2, D-1, and D-2. The configuration changes discussed herein comprised changes in the flame holders, changes in the fuel-injection pattern, and installation of a cooling liner. A summary of the pertinent features and dimensions is given in table I. The afterburner shell diameter was about $32\frac{1}{2}$ inches at the locations where flame holders were installed and 29 inches at the exhaust-nozzle inlet. The variable-area exhaust nozzle was about $8\frac{3}{4}$ inches long in the open position and could be varied from an area of 460 square inches to 302 square inches. No provision for cooling other than free convection and radiation to the tunnel walls was provided on the outside of the afterburner shell.

[redacted]

The cooling liner was constructed of 0.063-inch Inconel and extended from the flame-holder location to the exhaust-nozzle inlet. About 6 to 8 percent of the tail-pipe gas at turbine-outlet temperature flowed through the 1/2-inch passage between the liner and the shell. Cooling of the fixed portion of the variable-area nozzle was accomplished by the use of a double-wall construction with a small quantity of air from the compressor discharge flowing between the walls.

V-gutter-type flame holders were used throughout the investigation in conjunction with the center pilot. Cross sections of the three flame holders and the distribution of flame-seat area are shown in figure 2. The flame-holder blocked area varied from 24.6 to 40.6 percent of the combustion-chamber cross-sectional area. The clearance dimension from the flame holder to the burner shell varied from $2\frac{7}{8}$ to $4\frac{1}{2}$ inches. Flame-holder locations are given in table I.

Fuel injection was accomplished by two sets of radial spray bars (except for configuration B-2) similar to those described in reference 2. For configuration B-2, the secondary spray bars were replaced by a ring located 15 percent of the annular distance from the inner cone. Primary fuel was injected through the upstream set and secondary fuel, through the downstream set. A flow divider operating approximately on the schedule shown in figure 3 was used to maintain adequate fuel pressure for atomization at low flows without excessive fuel pressures at high fuel flows. It may be seen that at low total fuel-flow rates corresponding to high-altitude operation, most of the flow was injected through the primary bars.

The number of spray bars in each of the sets and the number of holes in the spray bars were varied as noted in table I and figures 4 and 5. A comparison of the fuel patterns of interest is presented in figures 4 and 5. For most configurations, the holes were drilled through both sides of the spray bars and fuel was injected normal to the direction of the gas flow. Each symbol therefore represents two orifices except for configuration C-2. Some of the holes in configuration C-2 were drilled in one side of the spray bar only and are denoted by the half-solid symbols. It should be noted that C-1 and D-2 were actually a single configuration which was common to two series.

Throughout the investigation MIL-F-5624 fuel was used in both the engine and afterburner. Autoignition of the afterburner fuel normally occurred as soon as the tail-pipe fuel-air ratio was increased to the range from about 0.02 to 0.04 because of the high (1275° F) turbine-outlet temperature maintained by the control. For ignition at extreme altitudes, a system was provided for momentarily increasing the fuel flow to one engine combustor. This momentary enrichment resulted in a burst of flame through the turbine into the afterburner, thereby igniting the afterburner fuel.

INSTRUMENTATION

Pressures and temperatures were measured at several stations in the engine proper and in the afterburner (fig. 6). Engine air flow was measured with survey rakes mounted at the engine inlet. A complete pressure and temperature survey was obtained at the turbine outlet, and total and static pressures at the afterburner outlet were measured with a water-cooled survey rake. Afterburner shell temperatures were measured by 11 thermocouples located at the exhaust-nozzle inlet as shown in figure 7. In order to obtain a correction to the scale thrust measurements, the drag of the water-cooled rake was measured by means of a pneumatic diaphragm mechanism.

PROCEDURE

Data were obtained over a range of afterburner fuel flows at the following simulated flight conditions:

Altitude (ft)	Flight Mach number	Configuration (see table I)									
15,000	0.19	A-1		A-3	B-1	B-2	B-3	C-1	C-2	D-1	D-2
25,000	.19	A-1	A-2	A-3	B-1	B-2	B-3	C-1		D-1	D-2
35,000	.19	A-1	A-2		B-1	B-2	B-3	C-1	C-2	D-1	D-2
45,000	.19						B-3	C-1	C-2	D-1	D-2
50-55,000	.19				B-1						

Dry refrigerated air was supplied to the engine at temperatures from about -10° to 20° F. No attempt was made to maintain standard inlet temperatures. The total pressure at the engine inlet was regulated to the value corresponding to the desired flight condition assuming complete free-stream ram pressure recovery.

At each flight condition with the engine operating at rated speed and temperature, the tail-pipe fuel flow was varied from a minimum determined by imminent blow-out to a maximum determined by (1) reaching the maximum exhaust-nozzle area, (2) attaining excessive shell temperatures, or (3) decreasing exhaust-gas temperature with increasing fuel flow.

Thrust measurements were obtained from the tunnel balance scales. Exhaust-gas temperatures and combustion efficiencies were obtained by the methods described in the appendix. Because of a nonuniform circumferential total-pressure distribution at the exhaust-nozzle outlet (station 8), absolute values of combustion efficiency are believed to be slightly higher than the true value; however, the validity of comparisons among configurations is not affected.

[redacted]

RESULTS AND DISCUSSION

During experimental investigations in the altitude wind tunnel, afterburner shell temperatures from 1200° to 1700° F have been common and have caused little damage. Such temperatures, however, may not be tolerated in flight applications where additional stresses due to maneuver loads are superimposed. No generally accepted limit for shell temperature has yet been determined; the value chosen will, of course, depend on the stresses imposed and on the properties of the materials.

Cursory inspection of the shell temperature changes reported herein might give the impression that these changes are unimportant; however, when considered in terms of the strength of available materials, these changes of from 50° to 200° F become significant. This significance is illustrated in figure 8 by strength-temperature curves for two typical afterburner materials, Inconel and Inconel X. The strengths of both materials may be seen to be extremely sensitive to changes in temperature in the range between 1000° and 1800° F. For example, a reduction from 1300° to 1200° F increases the tensile strength of Inconel from about 45,000 to 64,000 pounds per square inch, or about 42 percent.

Typical afterburner shell temperature distribution patterns in the plane of the exhaust-nozzle inlet are given in figure 9. Large temperature gradients may well exist between adjacent thermocouples. However, inasmuch as the temperature pattern shown persisted throughout the investigation irrespective of configuration changes, the trends shown are valid. Average temperature values are given for all succeeding figures, and it should be noted that peak temperature values may be more than 200° F hotter than the average. The irregular temperature may be associated with variations in local fuel-air ratio due to an irregular gas velocity pattern at the burner inlet.

It is reasonable to assume that the cooling problem may be alleviated by control of the radial distribution of exhaust-gas temperature in the critical region near the exhaust nozzle. For example, for a mean bulk exhaust-gas temperature of 3400° R, lower shell temperatures would be expected with a temperature profile ranging from about 3000° R near the shell to 3800° R near the center than for a uniform temperature of 3400° R. Two possible methods of controlling the exhaust-gas temperature distribution are (1) by variations in the radial or axial distribution of flame-seat area, and (2) by maintaining a "buffer layer" of relatively cool gas along the inside of the shell. The insulating effect of such a buffer layer may be obtained in two ways. First, the radial fuel-injection pattern may be designed to inject all the fuel some distance from the wall, thereby preventing combustion near the shell. Because of the very strong turbulence in the combustion chamber, a rather thick layer of gas must be left fuel-free with the result that a large portion of the air theoretically available for combustion cannot be utilized. This method of securing cooling by fuel stratification

restricts the maximum value of mean bulk exhaust-gas temperature obtainable. Secondly, preservation of the buffer layer can be ensured by the use of a liner which, with the shell, forms an annular passage through which a small fraction of the relatively cool gas leaving the turbine may flow. Inasmuch as only about 6 percent of the air passes through the cooling passage, more air is available for combustion, and higher mean bulk exhaust-gas temperatures are possible than by the use of variation in the radial fuel pattern.

Three configurations, which were alike with the exception of the flame holders, were investigated to determine the effect of flame-seat-area distribution on shell temperatures. The distribution of flame-seat area and the clearance dimension from the flame holder to the shell are shown in figure 2. The effects of these changes are given in figure 10 where the average shell temperature is shown as a function of exhaust-gas temperature, and in figure 11 where several afterburner performance variables are given as a function of fuel-air ratio.

The data of figure 10 show that an increase in the clearance dimension from $2\frac{7}{8}$ to $3\frac{11}{16}$ inches (changing from configuration A-1 to A-2) resulted in a reduction of as much as 130° F in shell temperature and a further increase to $4\frac{1}{2}$ inches (configuration A-3) again increased the shell temperatures to a value slightly above the original. It therefore appears that within the range investigated changes in the clearance dimension alone do not have a predictable effect on shell temperatures. Part of the explanation may be that for a given exhaust-gas temperature, radiative heat transfer may be constant but changes in clearance dimension, gutter stagger, and gutter shape may alter the velocity profiles and thus vary the convective heat transfer.

Augmented thrust ratio, specific fuel consumption, tail-pipe combustion efficiency, and exhaust-gas temperature are given in figures 11 and 12 to show the effects of these changes in flame-seat area on afterburner performance. At an altitude of 25,000 feet (fig. 11), the performance obtained with configuration A-2, having a clearance of $3\frac{11}{16}$ inches, was slightly better than that obtained with A-1 or A-3. At 35,000 feet (fig. 12), A-2 also had better performance than A-1. These performance changes may not, however, be attributed to the changes in clearance dimension alone inasmuch as the flame-holder blocked area was also changed. The performance changes noted are believed to be due primarily to the change in blocked area, although the relative alinement of flame-seat area and fuel distribution pattern may also have had some effect. From this brief study, it appears that although no rules may be stated, some alleviation of the shell cooling problem is possible by attempting changes in flame-seat area distribution without sacrifice in performance.

Series B and C configurations were investigated to determine the extent to which shell temperatures could be reduced by varying the thickness of the layer of gas near the shell (or liner), which is free of fuel. The only difference between these two configuration series other than fuel systems was that series C had a cooling liner installed. As shown in figure 4, the fuel-injection orifice patterns for series B were restricted to a range within the inner 70 percent of the annulus width. Results obtained with series B configurations are given in figures 13 to 16. When the secondary spray bars of configuration B-1 were replaced with a fuel ring (B-2) which concentrated the secondary fuel orifices nearer the inside of the annulus, average shell temperatures were increased slightly at altitudes of 15,000 and 25,000 feet; however, the effect at 35,000 feet was negligible. Effects of changes in the secondary fuel system would naturally be less at high altitudes because of the smaller percentage of fuel flow going through the secondary fuel system at low total fuel-flow rates (fig. 3). The increase in shell temperatures is attributed to radial penetration of the fuel jets from the fuel manifold, causing some of the secondary fuel to burn near the shell.

Shell temperature was reduced as much as 75° F by concentrating the fuel orifice pattern within the inner 40 percent of the annulus width (configuration B-3). Shell temperatures were not obtained with B-3 at altitudes of 25,000 and 35,000 feet because of instrumentation difficulties.

The effects of these changes in fuel-injection pattern on afterburner performance parameters are given in figures 14, 15, and 16 as a function of tail-pipe fuel-air ratio for altitudes of 15,000, 25,000, and 35,000 feet, respectively. At all altitudes and over the entire range of fuel-air ratio, the performance obtained with the fuel manifold ring (B-2) was inferior to that of B-1. The decrease in tail-pipe combustion efficiency was between 0.05 and 0.10. At an altitude of 15,000 feet, the performance with configuration B-3 was equal to that of B-1 at low tail-pipe fuel-air ratios, but the combustion efficiency with B-3 was about 0.09 lower at a tail-pipe fuel-air ratio of 0.043. At altitudes of 25,000 and 35,000 feet, the performance obtained with configuration B-3 was slightly superior to that of B-1 over the range of fuel-air ratio covered.

From the results obtained with the B series of configurations, it appears that the shell temperatures can be reduced significantly by control of radial fuel distribution, although the simultaneous effect on performance is uncertain. For example, the performance of configuration B-3 at an altitude of 15,000 feet might have been improved by the use of a flame holder better matched to the radial fuel distribution pattern.

[redacted]

Although the use of a cooling liner ensures the existence of a layer of relatively low-temperature gas along the inside of the burner shell, the heat transferred to the shell may nevertheless be affected by the temperature profile in the combustion chamber. The effect of changes in radial fuel distribution (and therefore temperature profile) on shell temperatures is given in figure 17 for configurations C-1 and C-2, which incorporated a cooling liner as shown in figure 1. The radial fuel patterns used are shown in figure 5. For configuration C-1 the fuel pattern covered the inner 57 percent of annulus width, whereas for C-2 the pattern covered the inner 70 percent.

As shown in figure 17, the outward shift in fuel pattern caused an increase of as much as 140° F in shell temperature. At all altitudes the increase in shell temperature became greater as the exhaust-gas temperature was raised.

The performance of these configurations (figs. 18 and 19) followed the expected trend with higher combustion efficiency being obtained at low fuel-air ratios with the more concentrated fuel pattern C-1 and the reverse being true at tail-pipe fuel-air ratios above about 0.035. It may be concluded from these figures that the introduction of fuel into the outer 40 percent of the annulus width will increase shell temperatures materially, but such fuel injection is necessary to obtain maximum thrust augmentation.

The effects of installing a cooling liner on both shell temperature and performance are given in figures 20 and 21 for configurations D-1, which had no liner, and D-2, which had a full-length liner. These configurations were otherwise identical. From figure 20, it will be seen that the use of a liner reduced the shell temperature as much as 200° F at a given exhaust-gas temperature. Liner temperatures were, of course, much higher than the shell temperatures shown; however, very high liner temperatures can be tolerated inasmuch as the stresses in the liner are very low. The maximum allowable exhaust-gas temperature is approximately 3500° R when a cooling liner is used because of (1) excessive liner temperature and (2) the fact that a portion of the air theoretically available for combustion cannot be utilized.

The effects of installing a liner on performance are given in figure 21 for altitudes of 15,000 and 45,000 feet. With the exception of a single point at a fuel-air ratio of 0.059 at an altitude of 45,000 feet, no performance penalty was incurred by installation of the liner.

CONCLUDING REMARKS

It may be concluded from the data presented herein that substantial reductions in tail-pipe burner shell temperatures are possible by the use of a cooling liner without appreciable performance losses. In addition, reductions in shell temperature are also possible by control of the radial fuel distribution; however, the effects on performance are uncertain.

No direct trend of shell temperature with changes in clearance between the flame holder and the shell was obtained; some reduction in shell temperature, however, appears possible by trail-and-error variation of radial flame-seat distribution.

Lewis Flight Propulsion Laboratory
National Advisory Committee for Aeronautics
Cleveland, Ohio

APPENDIX - CALCULATIONS

Symbols

A	cross-sectional area, sq ft
B	thrust-scale balance force, lb
C_j	jet-thrust coefficient, ratio of scale jet thrust to rake jet thrust
D	external drag of installation, lb
D_r	drag of exhaust-nozzle survey rake, lb
F_j	jet thrust, lb
F_n	net thrust, lb
$F_{n,e}$	standard engine net thrust, lb
f/a	fuel-air ratio
g	acceleration due to gravity, 32.2 ft/sec^2
H	total enthalpy, Btu/lb
h_c	lower heating value of fuel, Btu/lb
P	total pressure, lb/sq ft absolute
p	static pressure, lb/sq ft absolute
R	gas constant, 53.4 ft-lb/(lb)(^oR)
T	total temperature, ^oR
T_w	shell temperature, ^oF
t	static temperature, ^oR
V	velocity, ft/sec
w_a	air flow, lb/sec
w_c	compressor leakage air flow, lb/sec

w_f fuel flow, lb/hr

w_f/F_n specific fuel consumption based on total fuel flow and net augmented thrust, lb/(hr)(lb thrust)

w_g gas flow, lb/sec

γ ratio of specific heats of gases

η_b combustion efficiency

η_e engine combustor efficiency

Subscripts:

e engine

g gas

j station at which static pressure of jet equals free-stream static pressure

m fuel manifold

n exhaust-nozzle outlet vena contracta

s scale, condition at which scale thrust was measured

t tail-pipe burner

x inlet duct at frictionless slip joint

0 free-stream condition

1 engine inlet

3 engine combustor inlet

6 turbine outlet or diffuser inlet

8 exhaust nozzle, 1 inch upstream of exhaust-nozzle fixed portion outlet

Methods of Calculation

Air flow. - Air flow at the engine inlet was determined by the following equation from pressure and temperature measurements obtained in the inlet annulus:

$$w_{a,1} = p_1 A_1 \sqrt{\frac{2\gamma_1 g}{(\gamma_1 - 1)Rt_1}\left[\left(\frac{P_1}{p_1}\right)^{\frac{\gamma_1 - 1}{\gamma_1}} - 1\right]}$$

Air flow at station 3 was obtained by taking into account the measured air leakage at the last stage of the compressor in the following manner:

$$w_{a,3} = w_{a,1} - w_c$$

Gas flow. - Gas flow through the engine was determined as

$$w_{g,6} = w_{a,3} + \frac{w_{f,e}}{3600}$$

Gas flow through the tail-pipe burner is

$$w_{g,8} = w_{a,3} + \frac{w_{f,e} + w_{f,t}}{3600}$$

Tail-pipe fuel-air ratio. - The tail-pipe fuel-air ratio used herein is defined as the weight flow of fuel injected into the tail-pipe burner divided by the weight flow of unburned air entering the tail-pipe burner. Weight flow of unburned air was determined by assuming that the fuel injected into the engine combustor was completely burned. By combining air flow, engine fuel flow, and tail-pipe fuel flow, the following equation for tail-pipe fuel-air ratio was obtained:

$$(f/a)_t = \frac{w_{f,t}}{3600\, w_{a,3} - \frac{w_{f,e}}{0.068}}$$

where 0.068 is the stoichiometric fuel-air ratio for the engine fuel.

Augmented thrust. - The augmented jet thrust was determined from the balance-scale measurements by the following equation:

$$F_j = F_{j,s} = B + D + D_r + \frac{w_{a,1} V_x}{g} + A_x(p_x - p_0)$$

[redacted]

The last two terms represent momentum and pressure forces on the installation at the slip joint in the inlet air duct. The external drag of the installation was determined from experiments obtained with a blind flange installed at the engine inlet to prevent air flow through the engine.

The augmented net thrust was calculated by subtracting the free-stream momentum of the inlet air from the jet thrust of the installation as follows:

$$F_n = F_j - \frac{w_{a,1}}{g} V_0$$

Standard-engine thrust. - The jet thrust obtainable with the standard engine at rated engine speed was calculated as follows from measurements of turbine-outlet total pressure and temperature and gas flow obtained during the tail-pipe burning program:

$$F_{j,e} = C_j \left(\frac{w_{g,8}}{g} V_n + A_n (p_n - p_0) \right)$$

where the subscript n denotes the condition of the gas at the nozzle exit. The charts in reference 5 were used in the solution of the preceding equation.

Experimental data from previous operation of the engine indicated that the total-pressure loss across the standard-engine tail pipe between stations 6 and the exhaust-nozzle outlet was approximately $0.04\ P_6$ at rated engine speed. The jet-thrust coefficient C_j determined from previous engine operation was 0.979.

The standard-engine net thrust was calculated by subtracting the free-stream momentum of the inlet air from the jet thrust of the standard engine, so that

$$F_{n,e} = F_{j,e} - \frac{w_{a,1}}{g} V_0$$

Exhaust-gas total temperature. - The total temperature of the exhaust gas was determined from scale jet thrust, exhaust-nozzle total pressure, and gas flow as follows:

$$T_j = \frac{g F_{j,s}^2}{C_j^2 w_{g,8}^2 R \left(\frac{2\gamma_8}{\gamma_8 - 1}\right) \left[1 - \left(\frac{p_0}{p_8}\right)^{\frac{\gamma_8 - 1}{\gamma_8}}\right]}$$

The coefficient C_j for the variable-area exhaust nozzle over the range of exhaust-nozzle pressure ratio investigated was 0.979. The ratio of specific heats γ_8 was based on an estimated value of temperature determined from tail-rake pressure measurements.

2297

Combustion efficiency. - Tail-pipe combustion efficiency was obtained by dividing the enthalpy rise through the tail-pipe burner by the product of the fuel flow and the lower heating value of the tail-pipe fuel:

$$\eta_b = \frac{3600 w_{g,8} \Delta H_{g,t}}{w_{f,t} h_{c,t}}$$

$$= \frac{3600 w_{a,3} H_a \Big]_{T_l}^{T_j} + w_{f,e} H_{f,e} \Big]_{T_m}^{T_j} + w_{f,t} H_{f,t} \Big]_{T_m}^{T_j} - \eta_e w_{f,e} h_{c,e}}{w_{f,t} h_{c,t} + w_{f,e} h_{c,e} (1-\eta_e)}$$

The fuel temperature T_m was constant at 540° R. The unburned engine fuel was taken into account in the determination of tail-pipe combustion efficiency in the manner indicated in the preceding equation.

REFERENCES

1. Jansen, Emmert T., and Thorman, H. Carl: Altitude Performance Characteristics of Tail-Pipe Burner with Variable-Area Exhaust Nozzle. NACA RM E50E29, 1950.

2. Conrad, E. William, and Prince, William R.: Altitude Performance and Operational Characteristics of 29-Inch-Diameter Tail-Pipe Burner with Several Fuel Systems and Flame Holders on J35 Turbojet Engine. NACA RM E9G08, 1949.

3. Johnson, LaVern A., and Meyer, Carl L.: Altitude Performance Characteristics of Turbojet-Engine Tail-Pipe Burner with Variable-Area Exhaust Nozzle Using Several Fuel Systems and Flame Holders. NACA RM E50F28, 1950.

[redacted]

4. Koffel, William K., Stamper, Eugene, and Sanders, Newell D.: Cooling of Ram Jets and Tail-Pipe Burners - Analytical Method for Determining Temperatures of Combustion Chamber Having Annular Cooling Passage. NACA RM E9L09, 1950.

5. Turner, L. Richard, Addie, Albert N., and Zimmerman, Richard H.: Charts for the Analysis of One-Dimensional Steady Compressible Flow. NACA TN 1419, 1948.

[redacted]

TABLE I - SUMMARY OF CONFIGURATION DETAILS

Series	Configuration	Flame holder					Fuel system				Burning length[1] (in.)	Cooling liner
		Type	Blocked area (percent)	Gutter angle (deg)	Shell clearance dimension (in.)	Location downstream of pilot (in.)	Primary		Secondary			
							Number of bars	Location[2] (in.)	Number of bars	Location[2] (in.)		
A	1	2-ring V	30.4	35,41	$2\frac{7}{8}$	$6\frac{3}{8}$	12	$20\frac{1}{8}$	12	$16\frac{1}{8}$	$65\frac{5}{8}$	None
	2	2-ring V	40.6	35	$3\frac{11}{16}$	$6\frac{3}{8}$	12	$20\frac{1}{8}$	12	$16\frac{1}{8}$	$65\frac{5}{8}$	None
	3	1-ring V	24.6	41	$4\frac{1}{2}$	$6\frac{3}{8}$	12	$20\frac{1}{8}$	12	$16\frac{1}{8}$	$65\frac{5}{8}$	None
B	1	2-ring V	30.4	35	$2\frac{7}{8}$	$8\frac{1}{2}$	20	$28\frac{1}{4}$	20	$24\frac{1}{4}$	63	None
	2	2-ring V	30.4	35	$2\frac{7}{8}$	$8\frac{1}{2}$	20	$28\frac{1}{4}$	fuel ring	$24\frac{1}{4}$	63	None
	3	2-ring V mounted on pilot cone	30.4	35	$2\frac{7}{8}$	$8\frac{1}{2}$	12	$29\frac{1}{4}$	12	$25\frac{1}{4}$	63	Diffuser only
C	1	2-ring V mounted on pilot cone	30.4	35	$2\frac{7}{8}$	$8\frac{1}{2}$	20	$28\frac{1}{4}$	20	$24\frac{1}{4}$	63	Full length
	2	2-ring V mounted on pilot cone	30.4	35	$2\frac{7}{8}$	$8\frac{1}{2}$	8	$28\frac{1}{4}$	12	$24\frac{1}{4}$	63	Full length
D	1	2-ring V mounted on pilot cone	30.4	35	$2\frac{7}{8}$	$8\frac{1}{2}$	20	$28\frac{1}{4}$	20	$24\frac{1}{4}$	63	Diffuser only
	2	2-ring V mounted on pilot cone	30.4	35	$2\frac{7}{8}$	$8\frac{1}{2}$	20	$28\frac{1}{4}$	20	$24\frac{1}{4}$	63	Full length

[1]Distance from flame holder to exhaust-nozzle outlet (open position).

[2]Distance forward of flame holder.

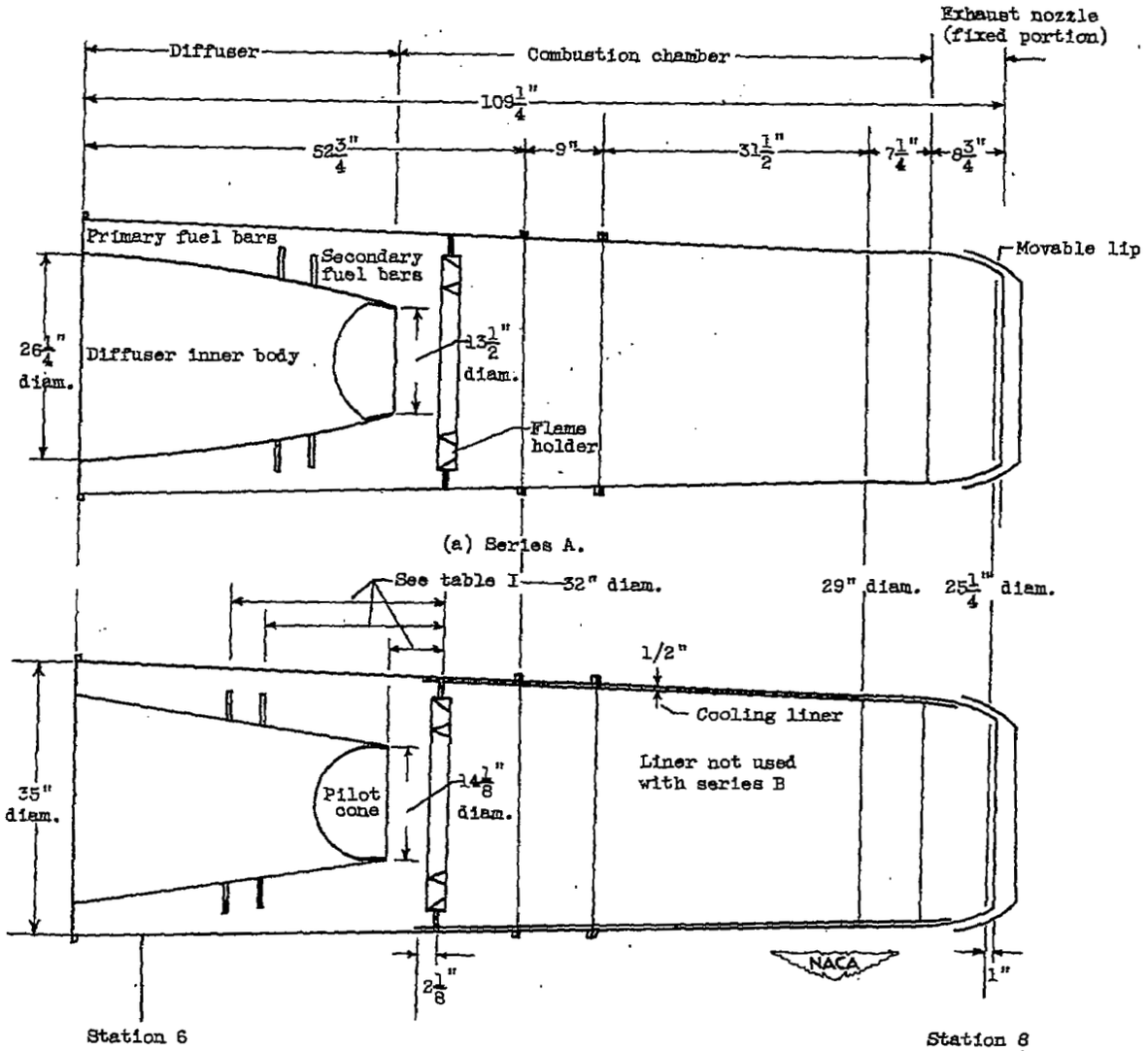

(b) Series B, C, and D.

Figure 1. - Schematic drawing of afterburner showing variation of diffuser inner body.

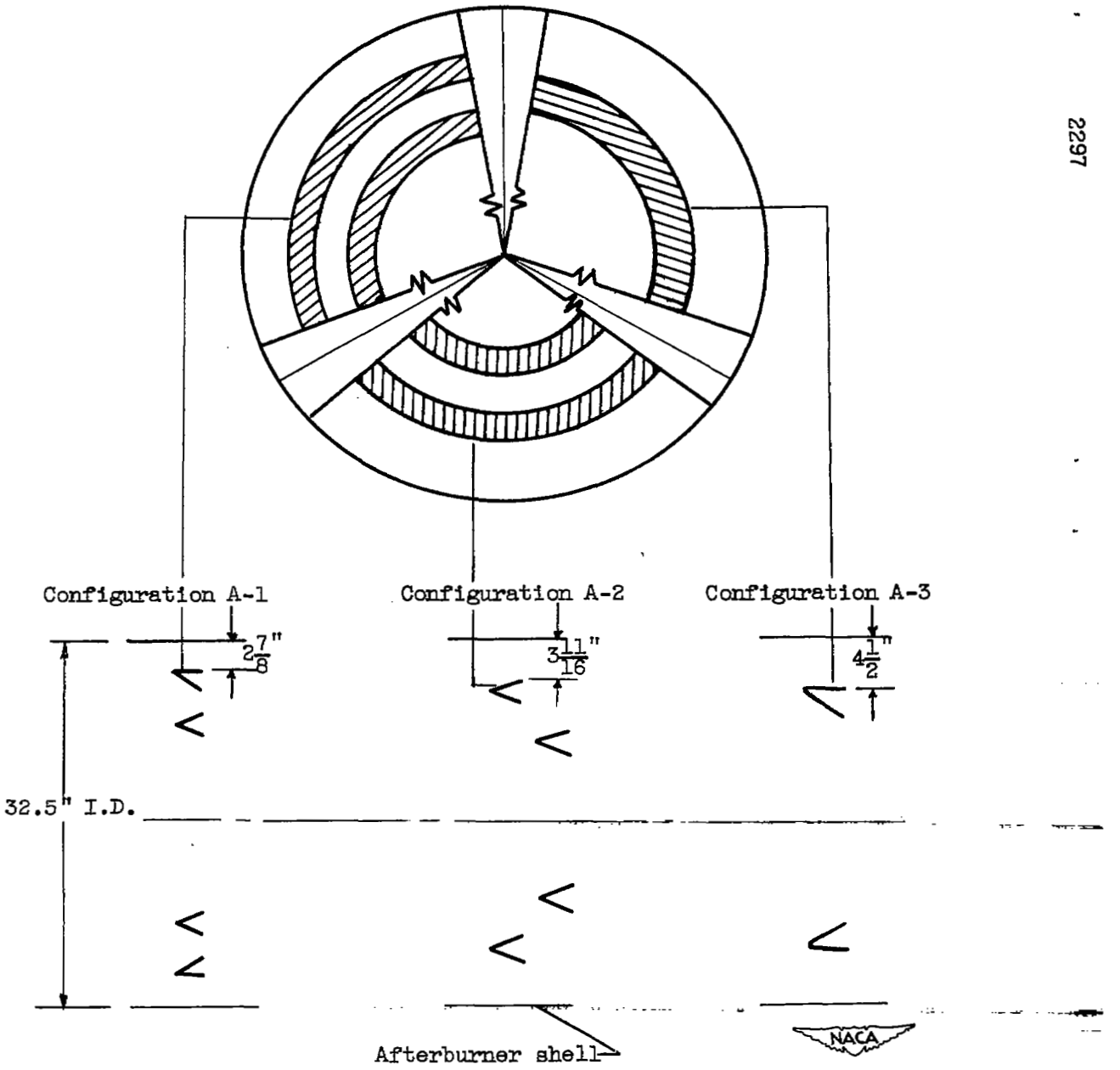

Figure 2. - Details of flame holders and distribution of flame-seat area.

[redacted]

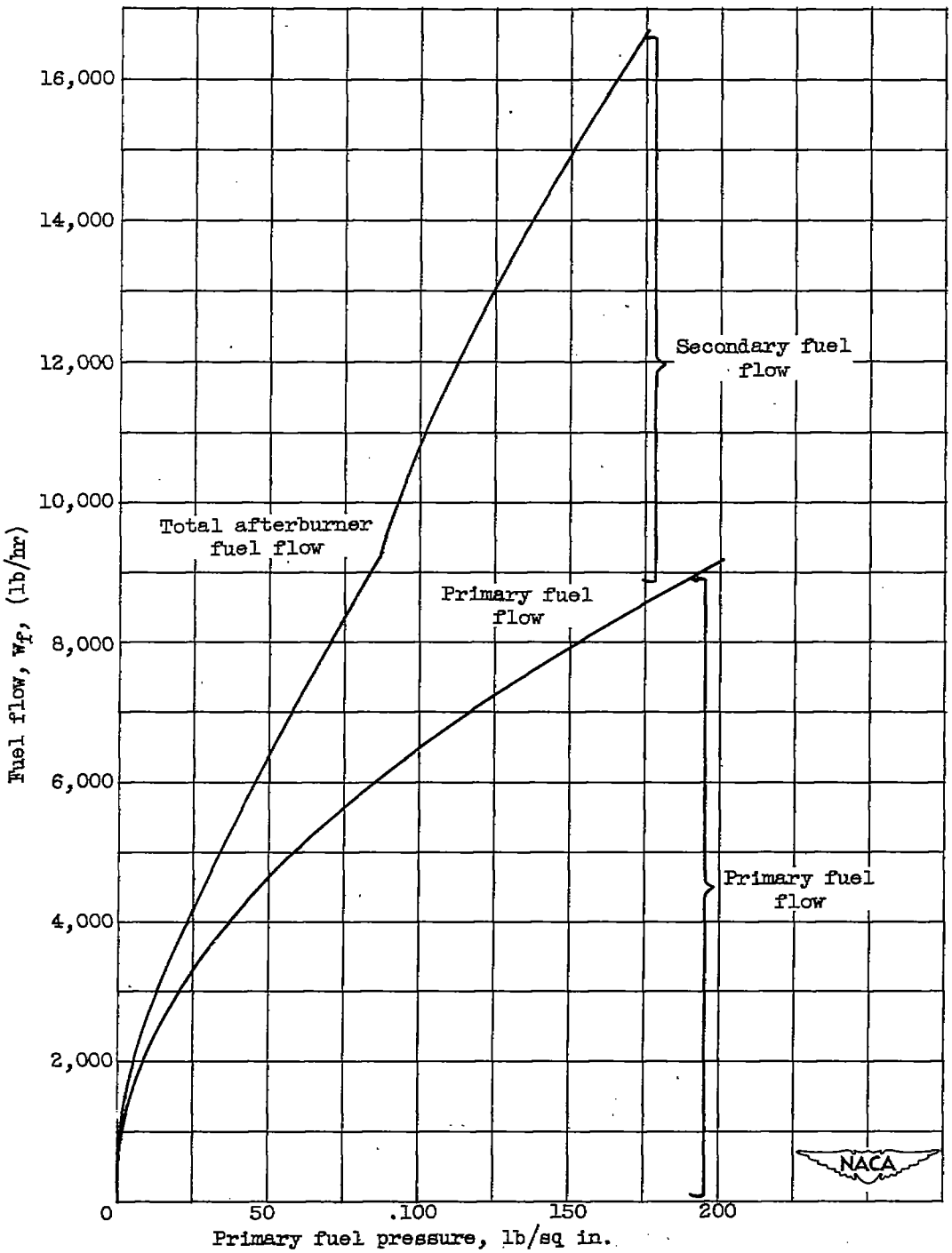

Figure 3. - Afterburner flow divider characteristics.

[redacted]

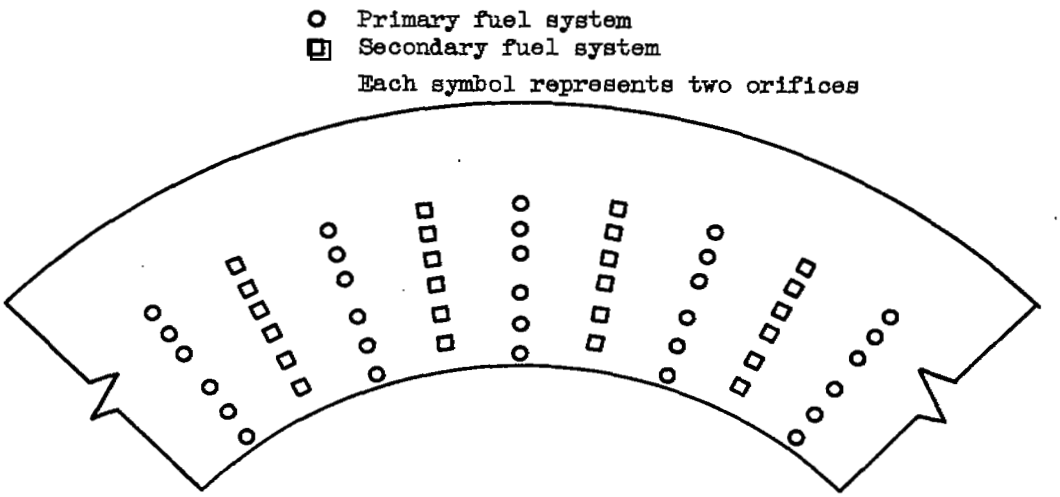

(a) Configuration B-1. Fuel orifice diameter, 0.020 inch.

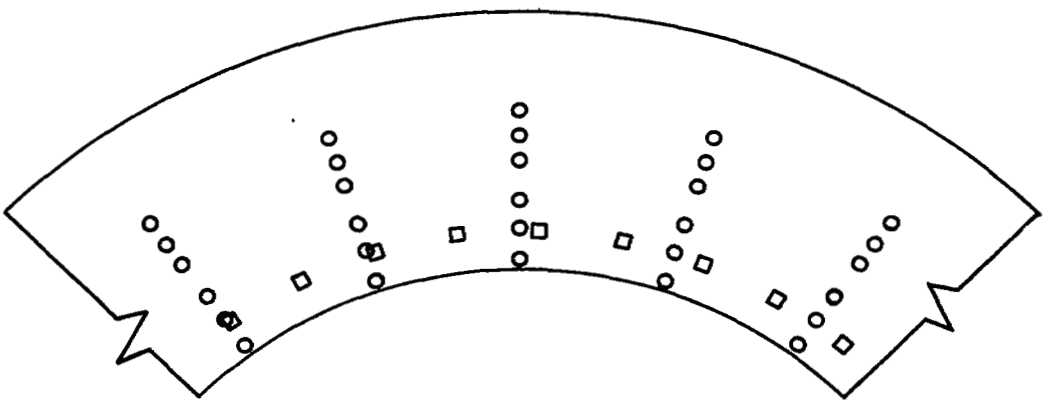

(b) Configuration B-2. Fuel orifice diameter, 0.020 inch for primary system and 0.035 inch for secondary system.

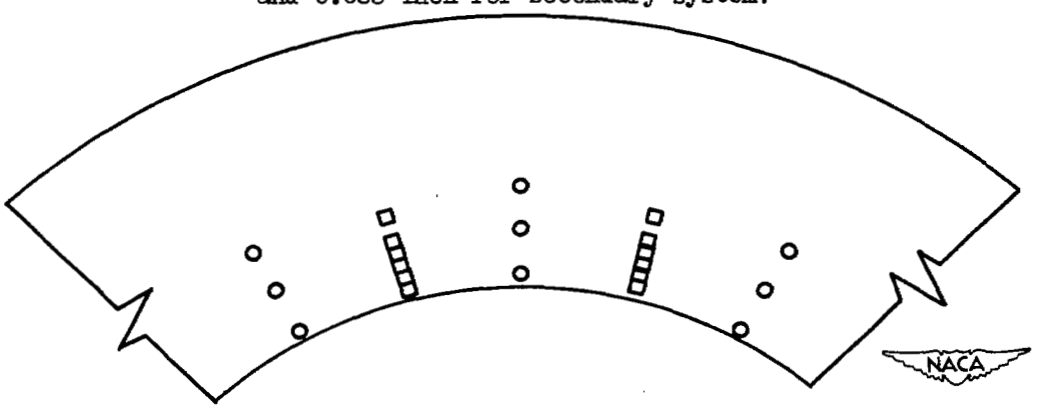

(c) Configuration B-3. Fuel orifice diameter, 0.030 inch.

Figure 4. - Details of fuel systems used with series B configurations.

[redacted]

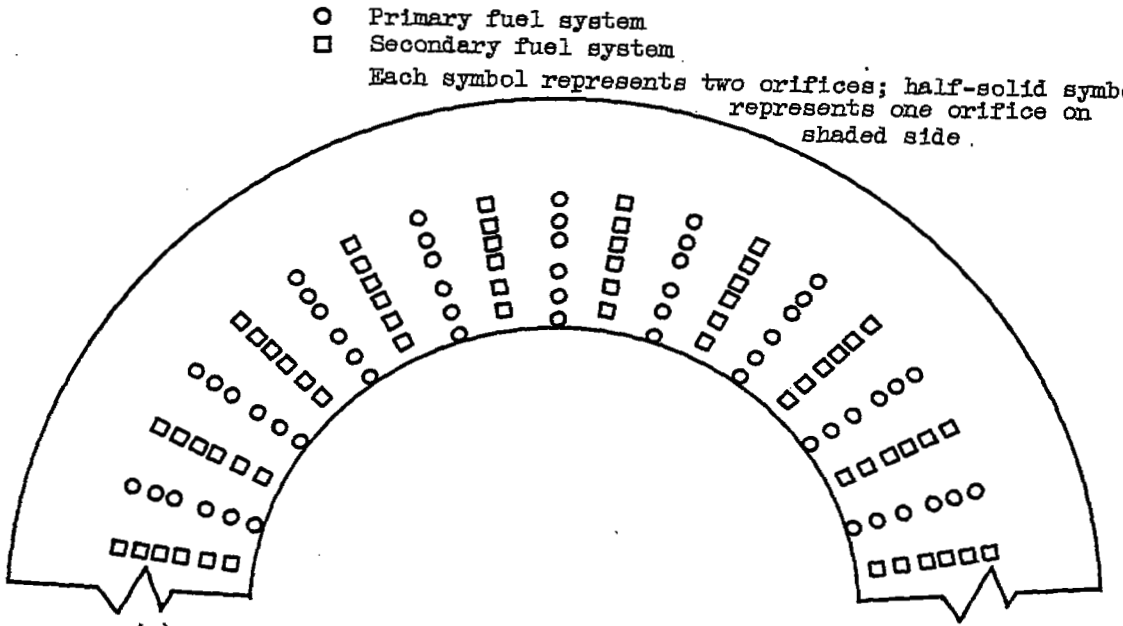

(a) Configuration C-1. Fuel orifice diameter, 0.020 inch.

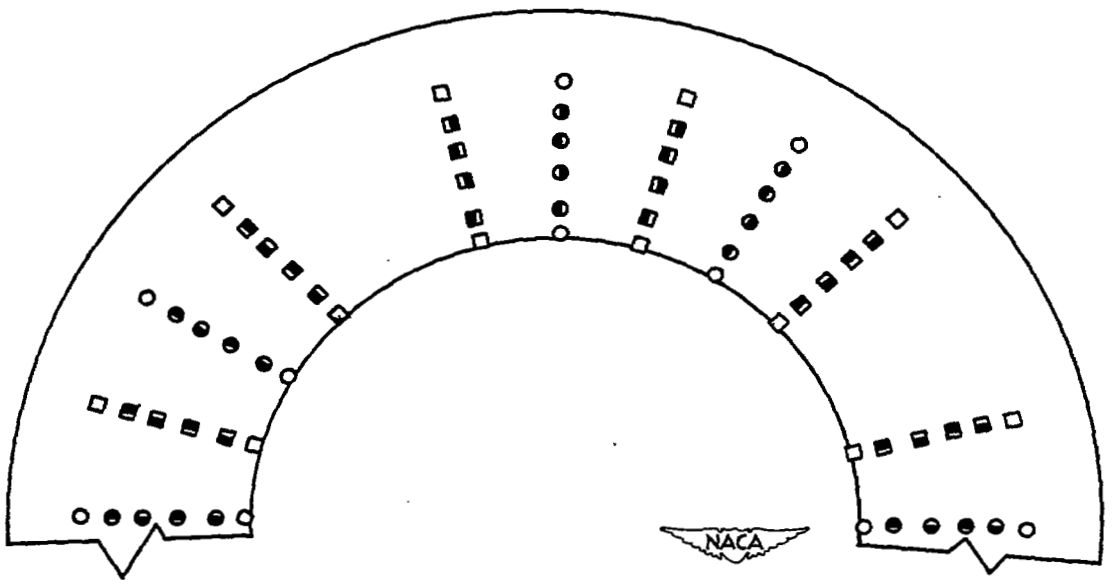

(b) Configuration C-2. Fuel orifice diameter, 0.030 inch.

Figure 5. - Details of fuel systems used with series C configurations.

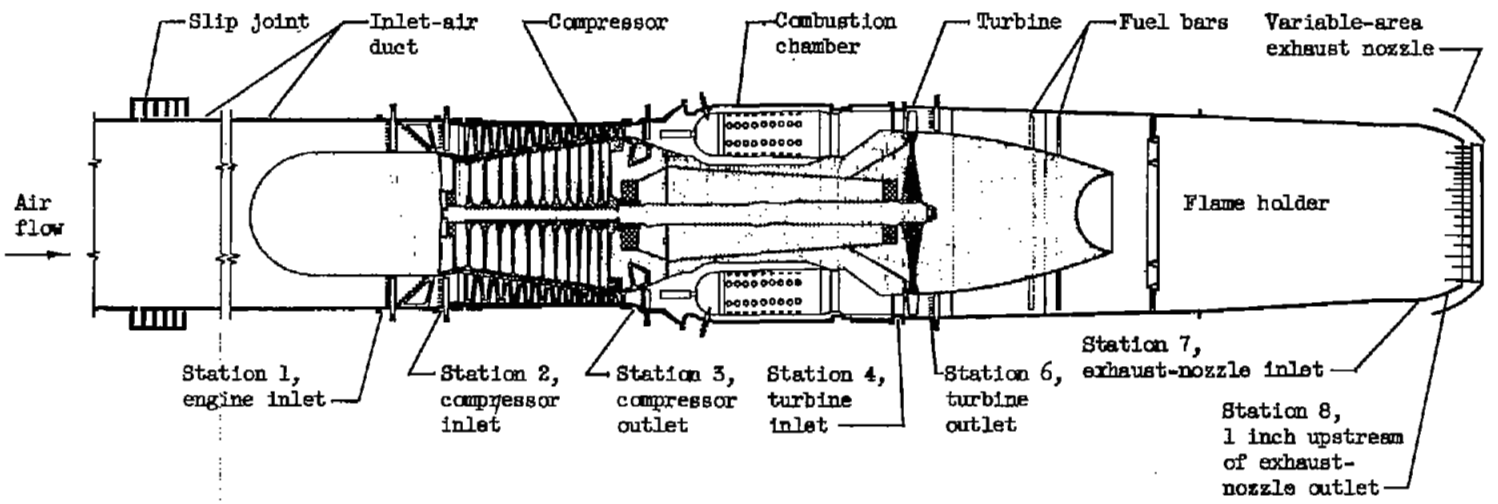

Station	Total-pressure tubes	Static-pressure tubes	Wall static-pressure orifices	Thermo-couples
1	32	8	5	4
2	6	0	2	0
3	20	0	4	6
4	5	0	0	0
6	30	0	4	24
7	0	0	0	11(skin)
8	20	3	4	0

Figure 6. - Cross section of turbojet-engine installation showing instrumentation.

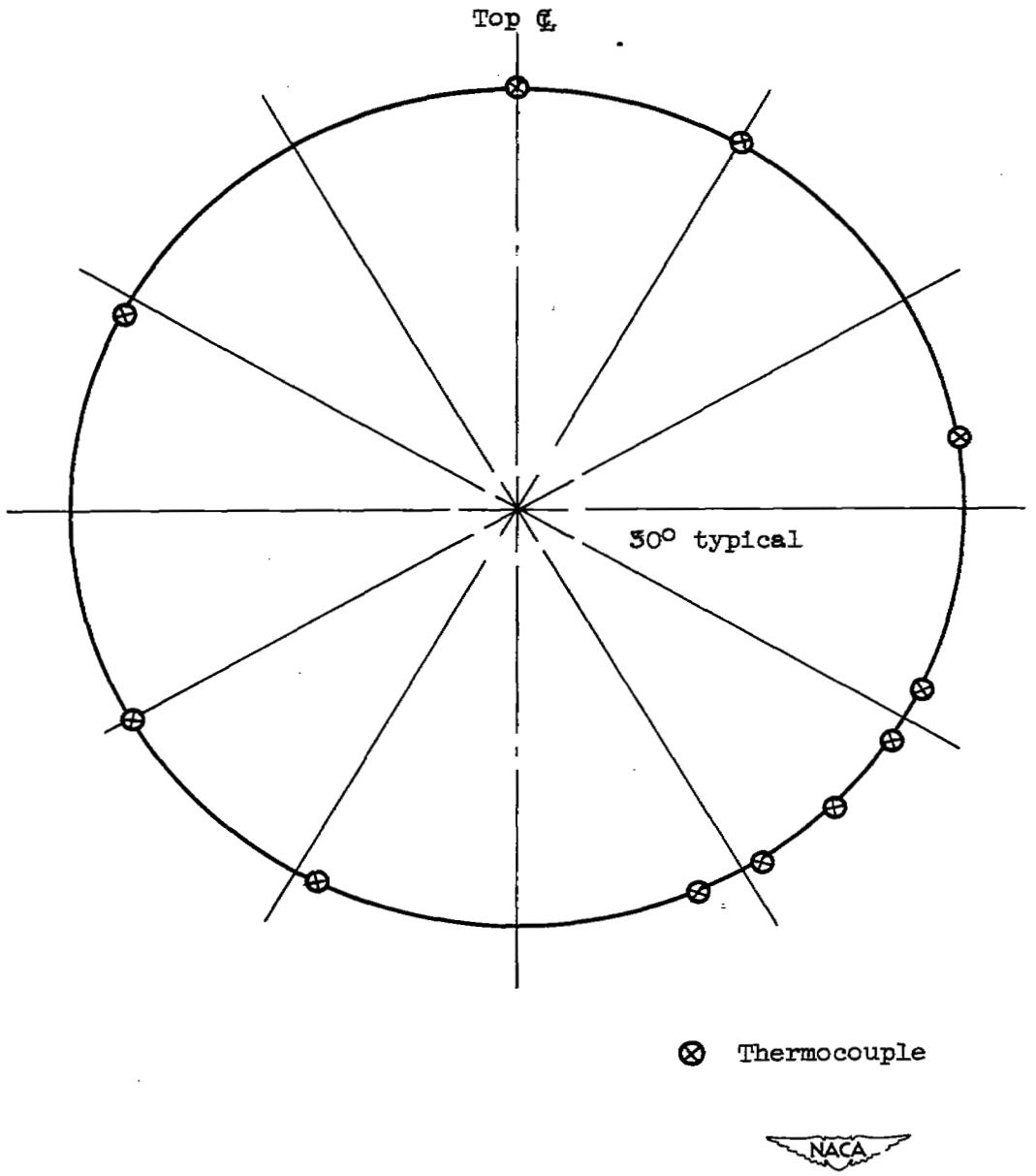

Figure 7. - Afterburner shell temperature survey at nozzle inlet (looking downstream) $11\frac{1}{2}$ inches ahead of nozzle outlet.

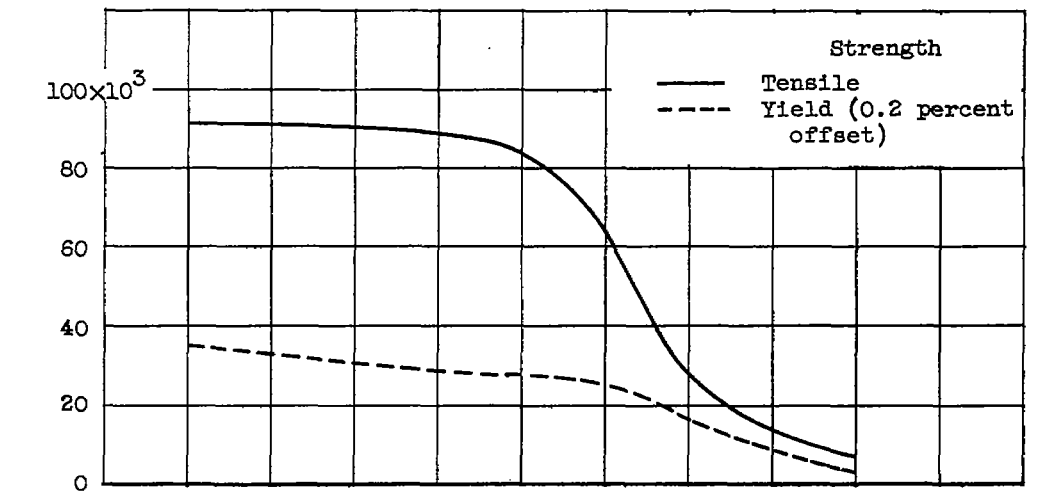

(a) Inconel.

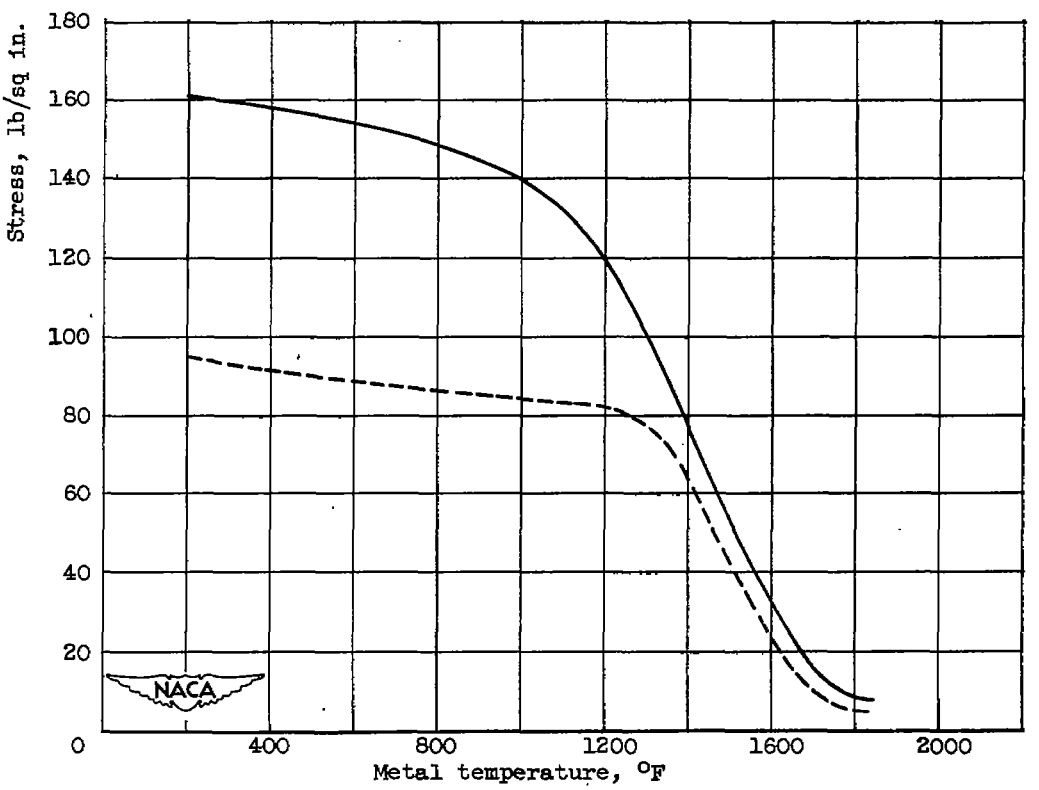

(b) Inconel X.

Figure 8. - Short-time high-temperature properties of oxidation-resisting alloys.

[redacted]

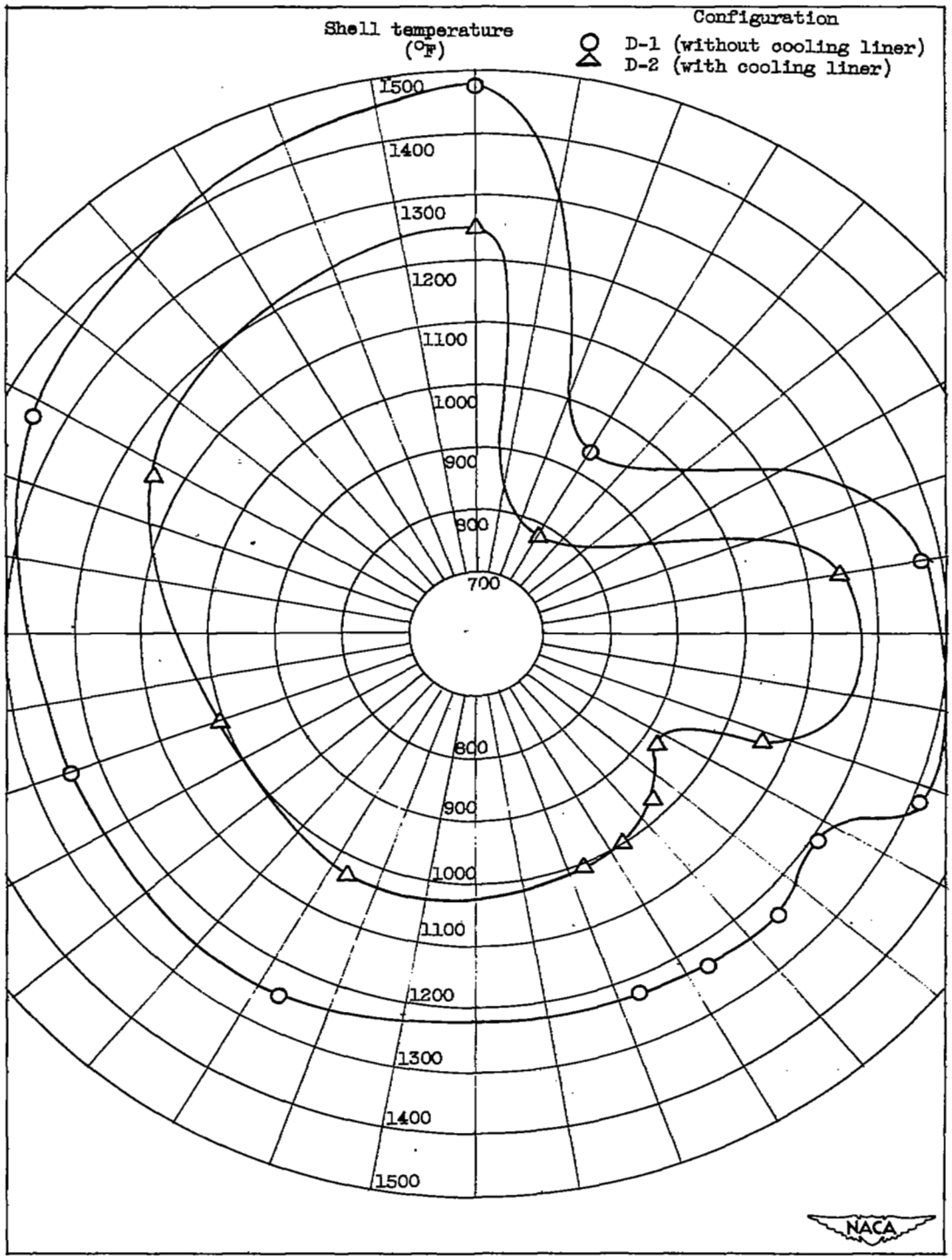

Figure 9. - Typical circumferential afterburner shell temperature profiles.

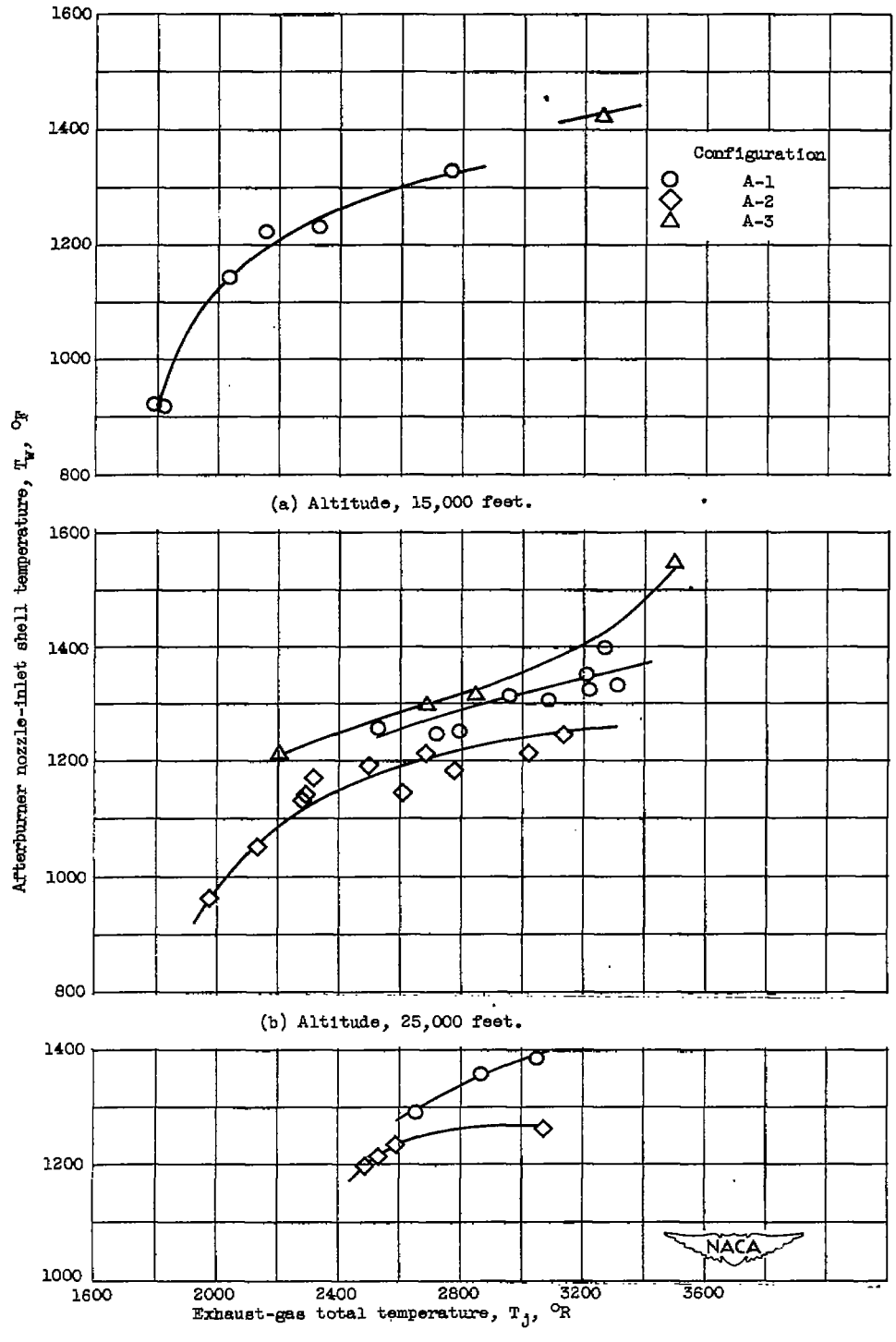

Figure 10. - Effect of exhaust-gas temperature on afterburner shell temperature for three flame-holder configurations.

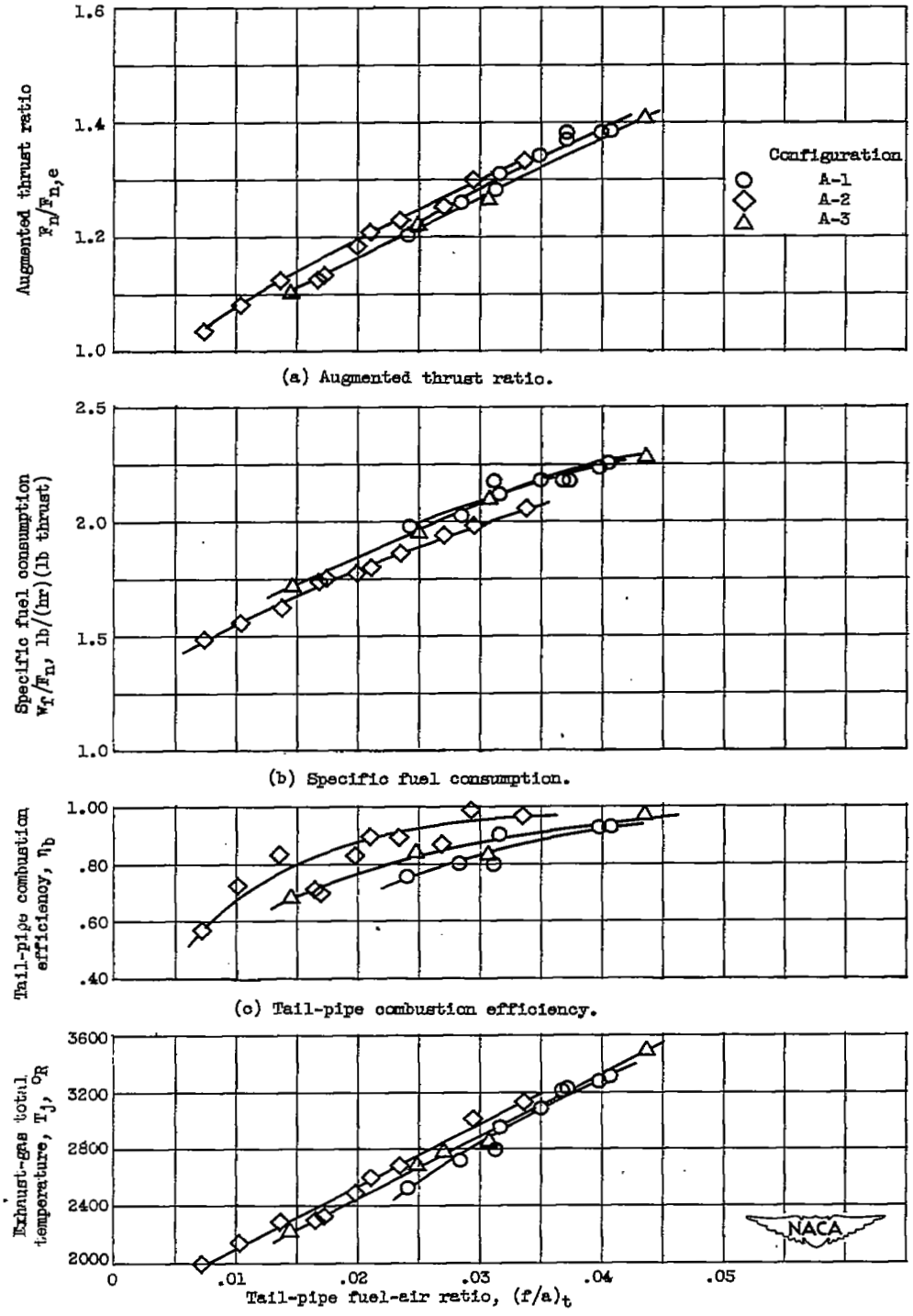

Figure 11. - Effect of flame-holder design on afterburner performance at altitude of 25,000 feet. Flight Mach number, 0.21; engine speed, 7900 rpm.

[redacted]

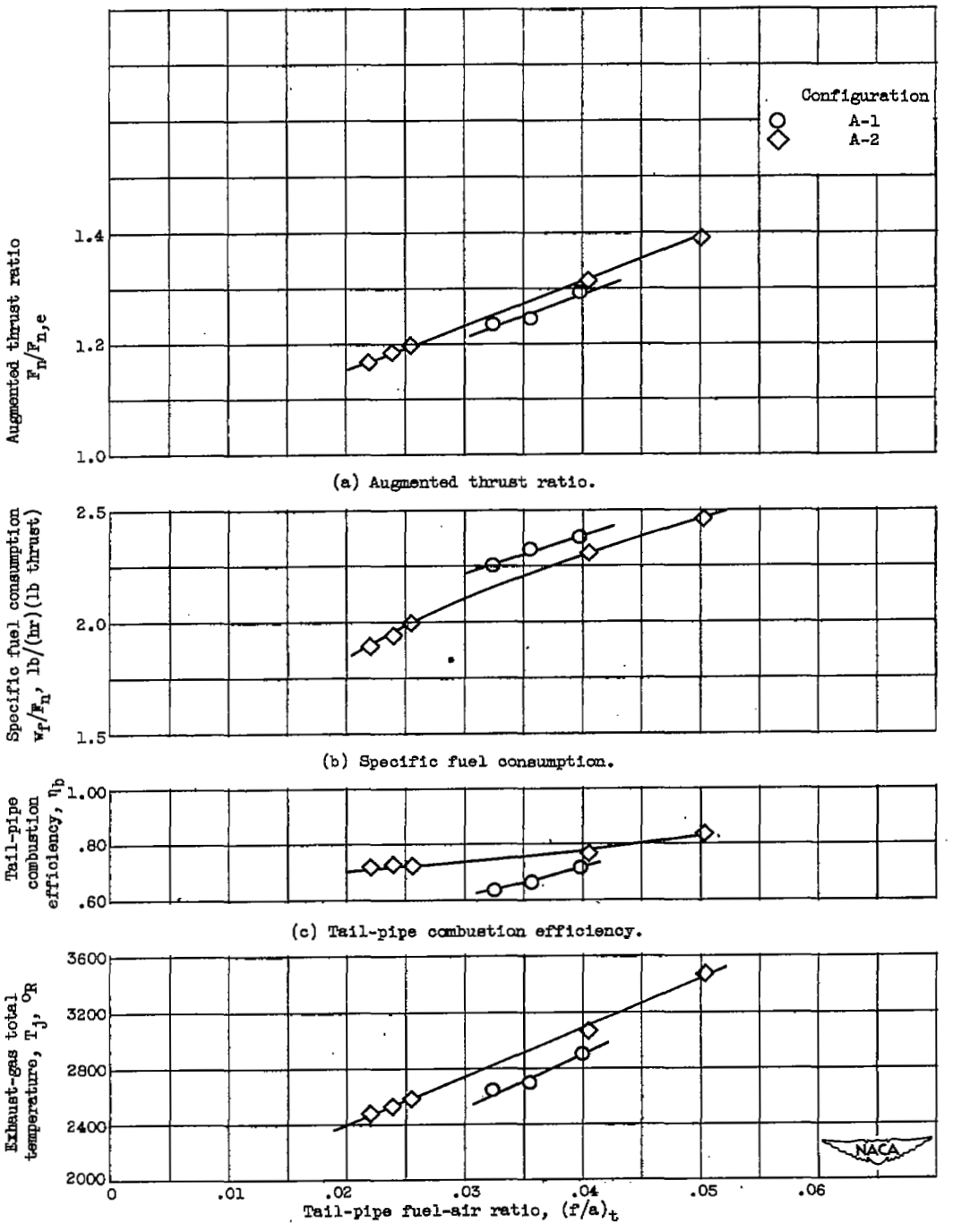

Figure 12. - Effect of flame-holder design on afterburner performance at altitude of 35,000 feet. Flight Mach number, 0.21; engine speed, 7900 rpm.

[redacted]

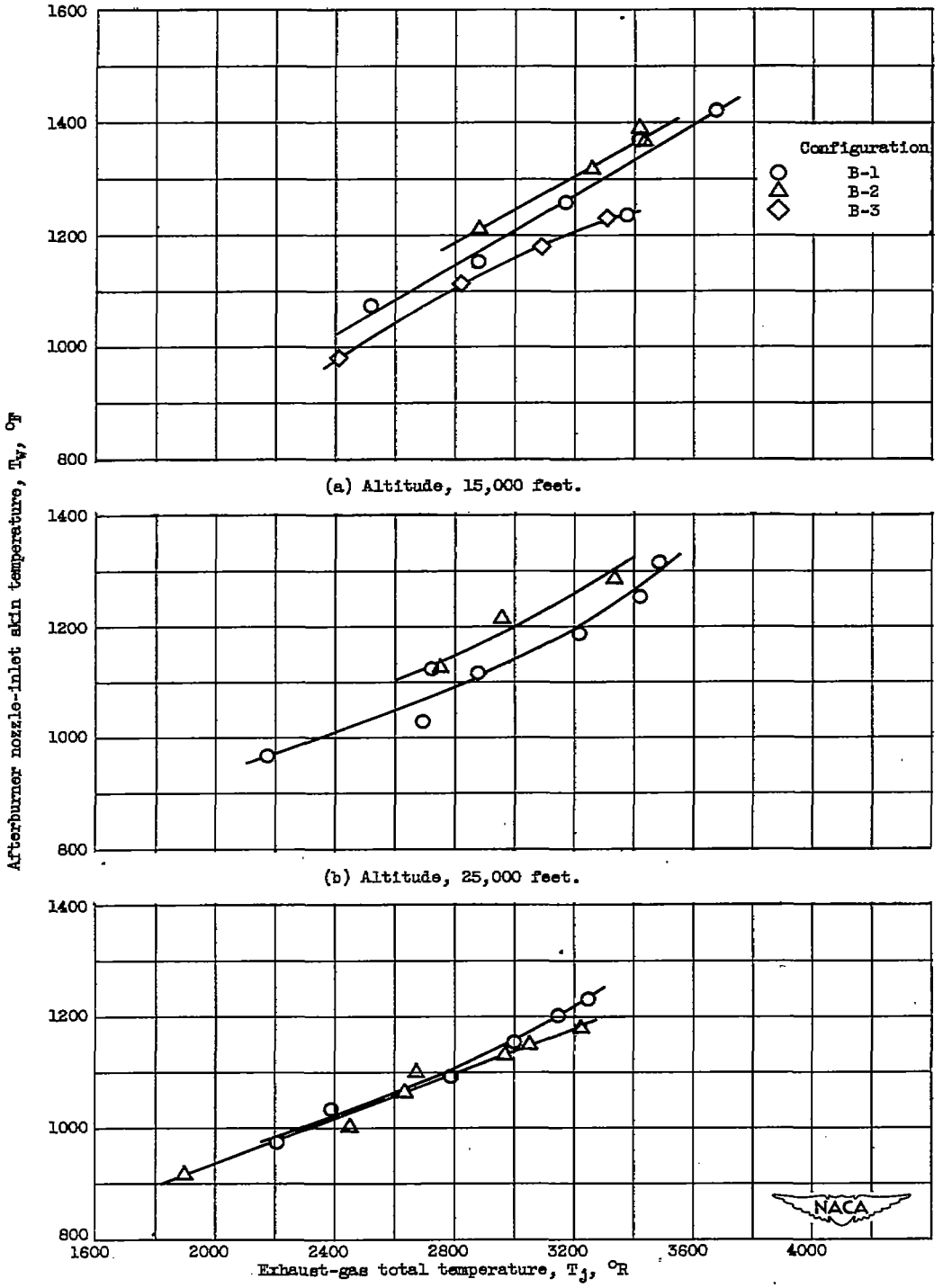

Figure 13. - Effect of exhaust-gas temperature on afterburner shell temperature for three fuel system configurations.

[redacted]

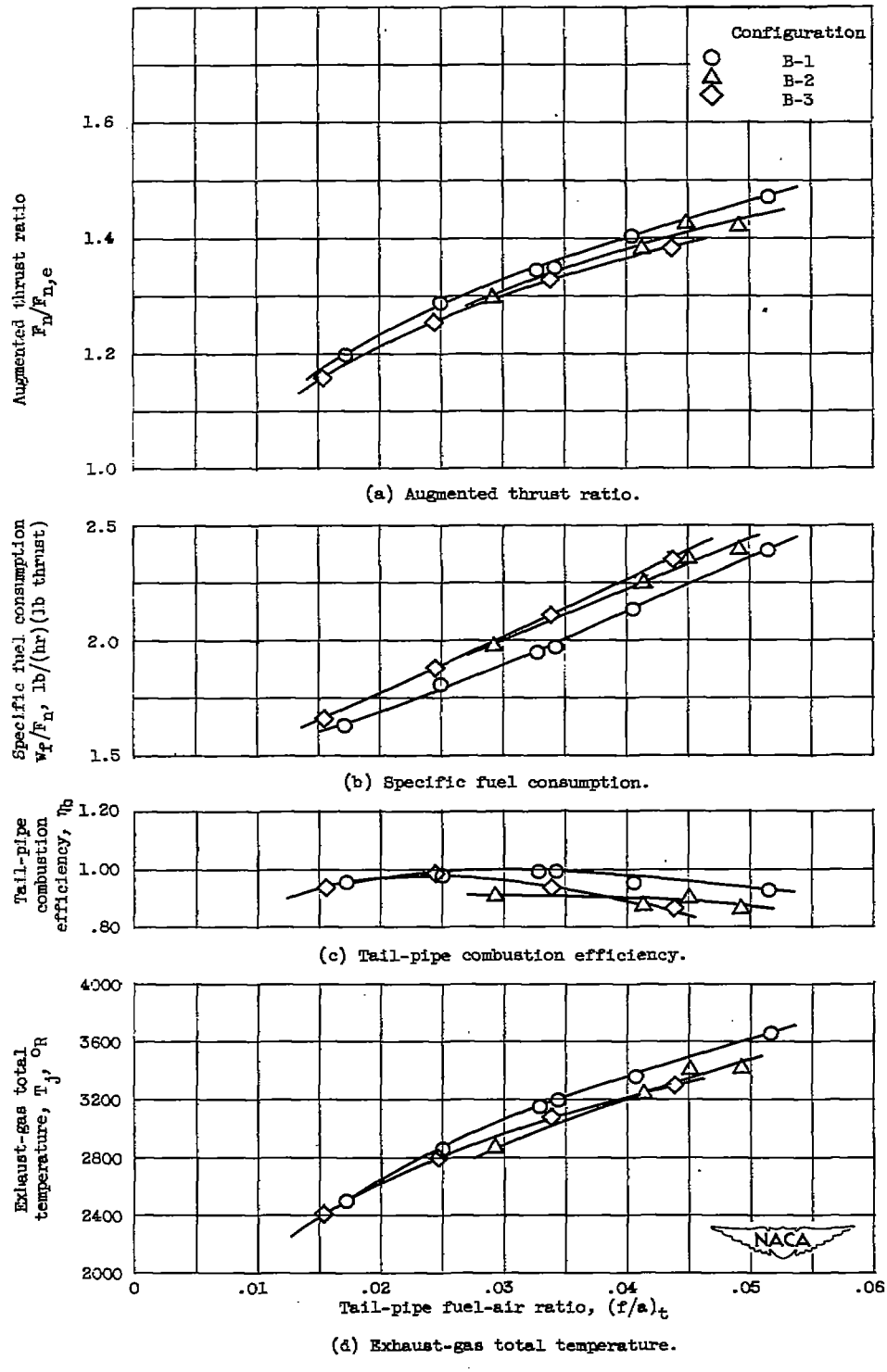

Figure 14. - Effect of fuel system pattern on afterburner performance at altitude of 15,000 feet. Flight Mach number, 0.21; engine speed, 7900 rpm.

[redacted]

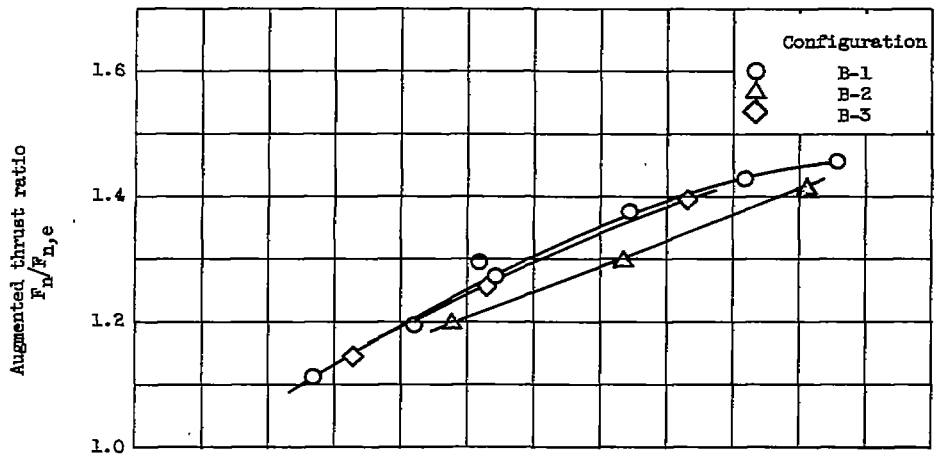

(a) Augmented thrust ratio.

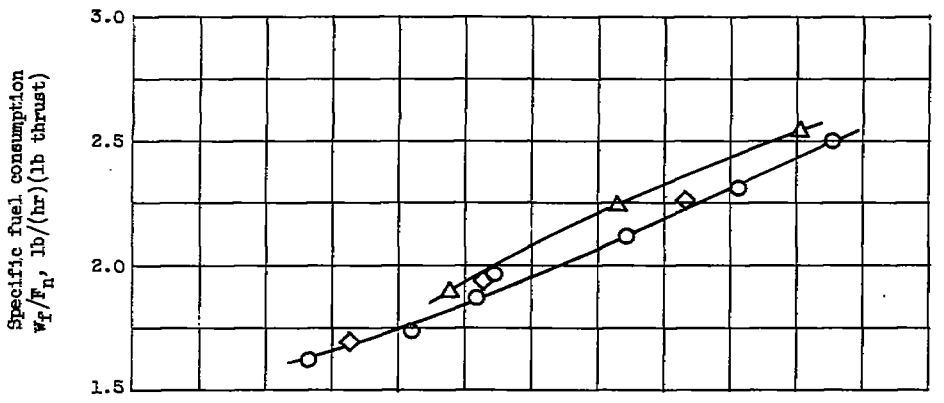

(b) Specific fuel consumption.

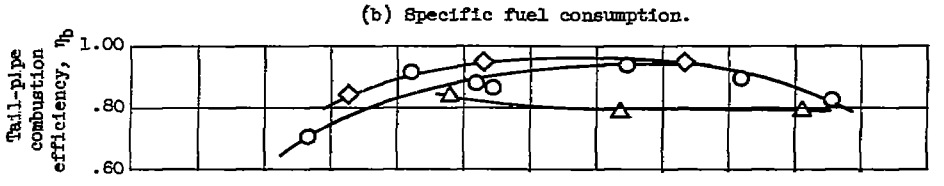

(c) Tail-pipe combustion efficiency.

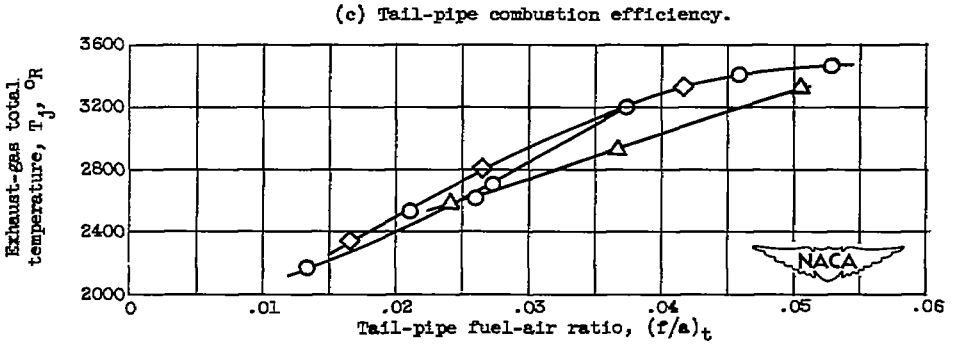

(d) Exhaust-gas total temperature.

Figure 15. - Effect of fuel system pattern on afterburner performance at altitude of 25,000 feet. Flight Mach number, 0.21; engine speed, 7900 rpm.

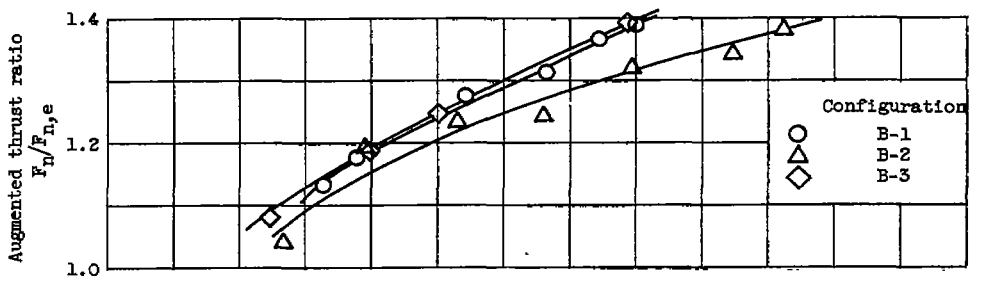

(a) Augmented thrust ratio.

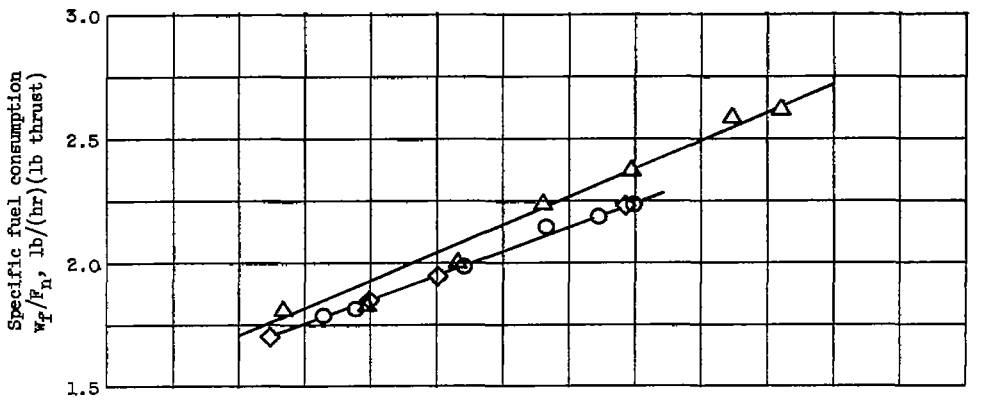

(b) Specific fuel consumption.

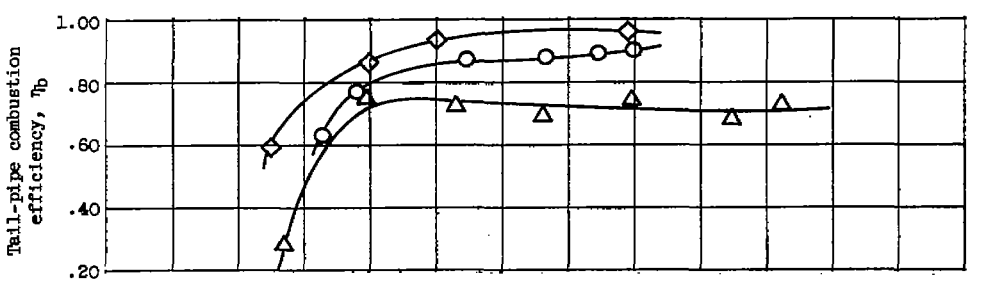

(c) Tail-pipe combustion efficiency.

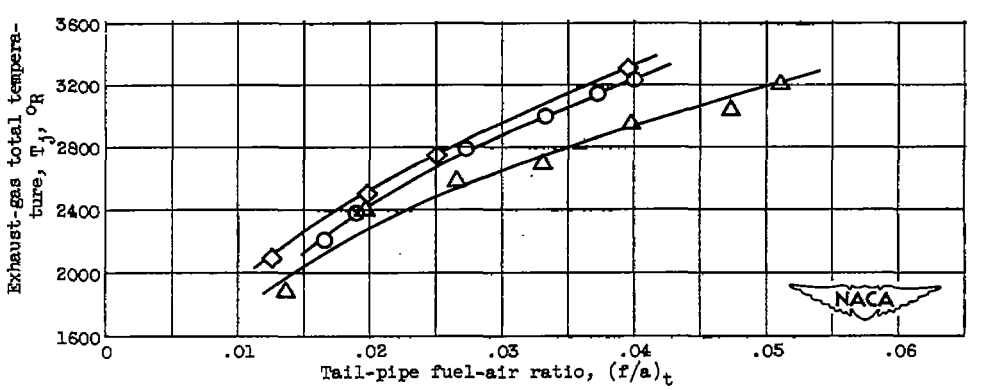

(d) Exhaust-gas total temperature.

Figure 16. - Effect of fuel system pattern on afterburner performance at altitude of 35,000 feet. Flight Mach number, 0.21; engine speed, 7900 rpm.

[redacted]

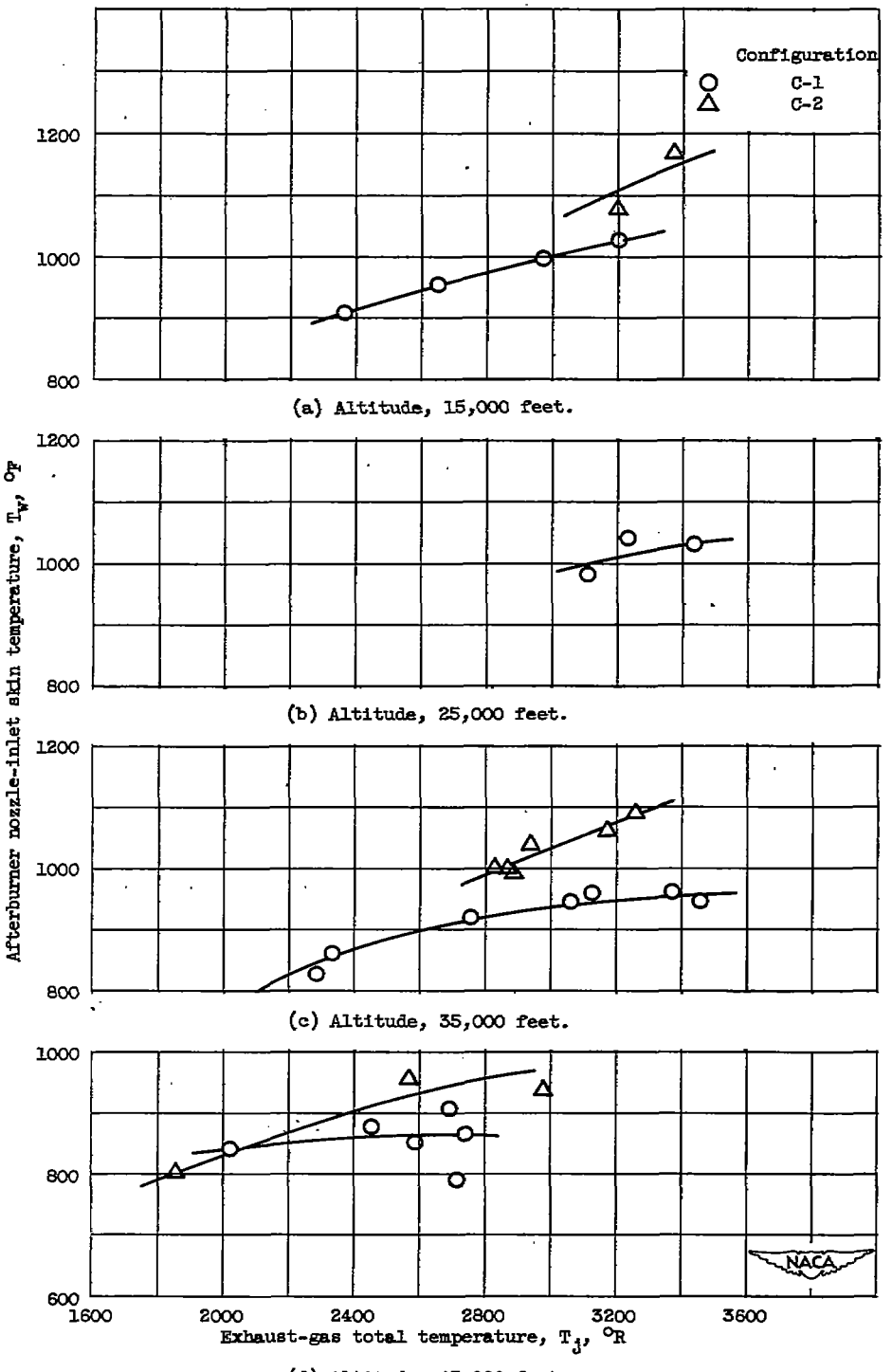

Figure 17. - Effect of exhaust-gas temperature on afterburner shell temperature for two fuel system configurations with a cooling liner installed.

[redacted]

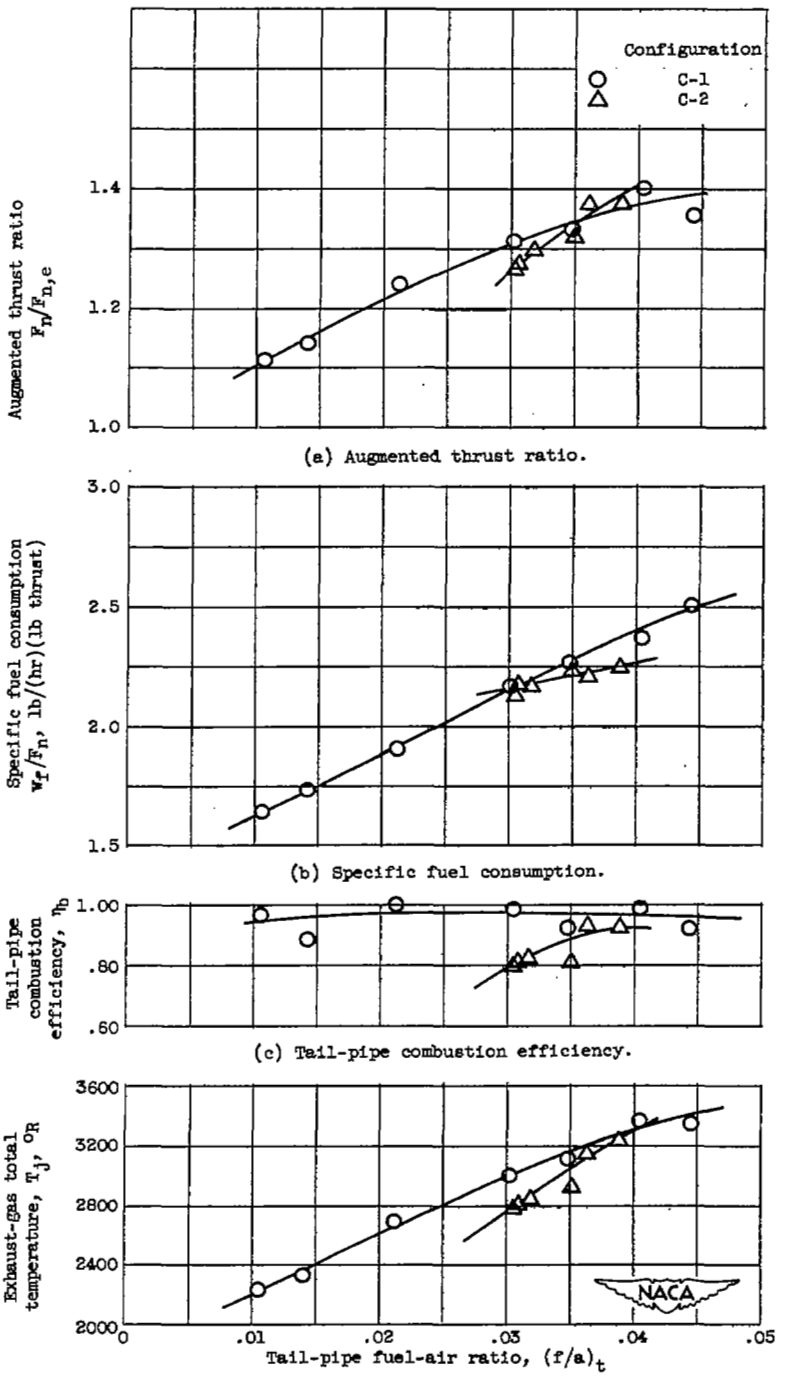

Figure 18. - Effect of fuel system pattern with a cooling liner installed on afterburner performance at altitude of 35,000 feet. Flight Mach number, 0.21; engine speed, 7900 rpm.

[redacted]

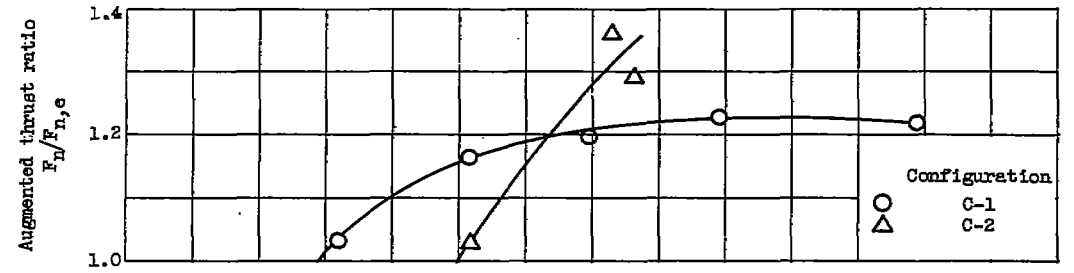

(a) Augmented thrust ratio.

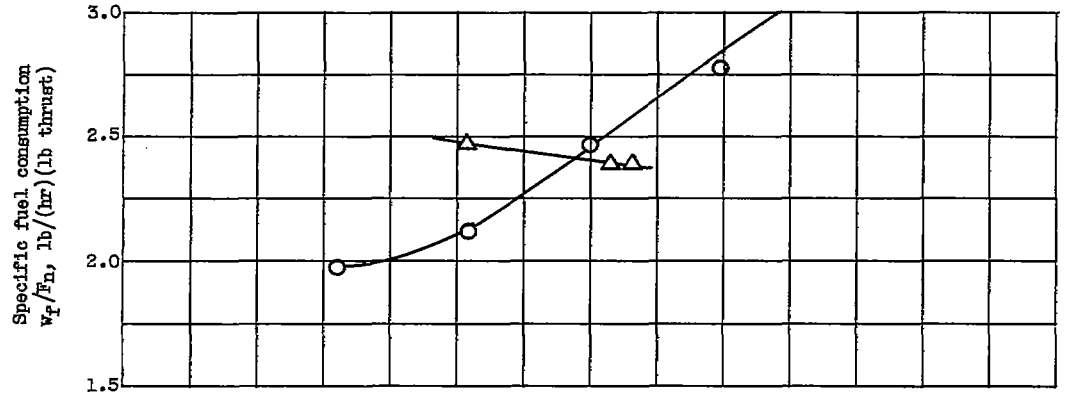

(b) Specific fuel consumption.

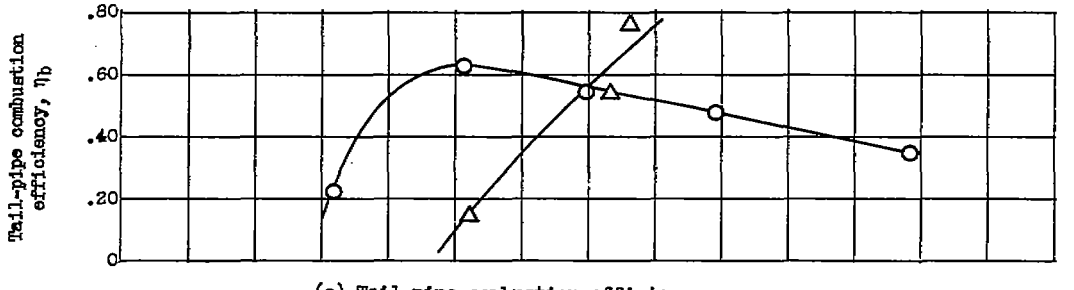

(c) Tail-pipe combustion efficiency.

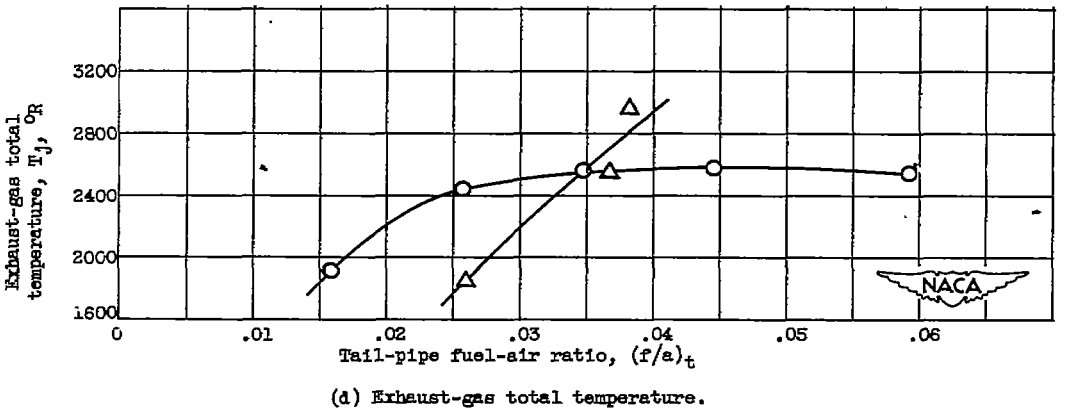

(d) Exhaust-gas total temperature.

Figure 19. - Effect of fuel system pattern with cooling liner installed on afterburner performance at altitude of 45, 000 feet. Flight Mach number, 0.21; engine speed, 7900 rpm.

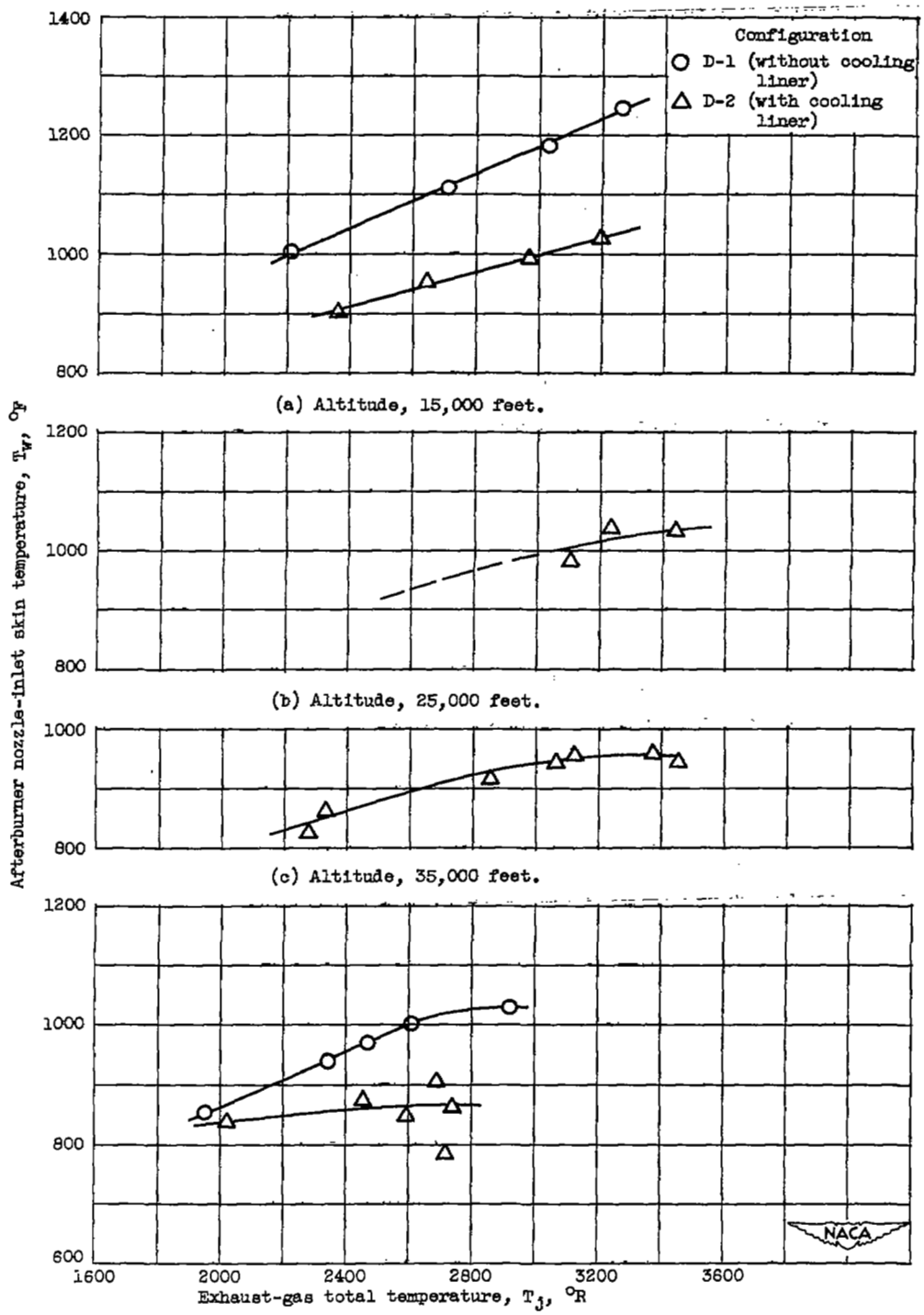

Figure 20. - Effect of exhaust-gas temperature on afterburner shell temperature for afterburner with and without cooling liner installed.

[redacted]

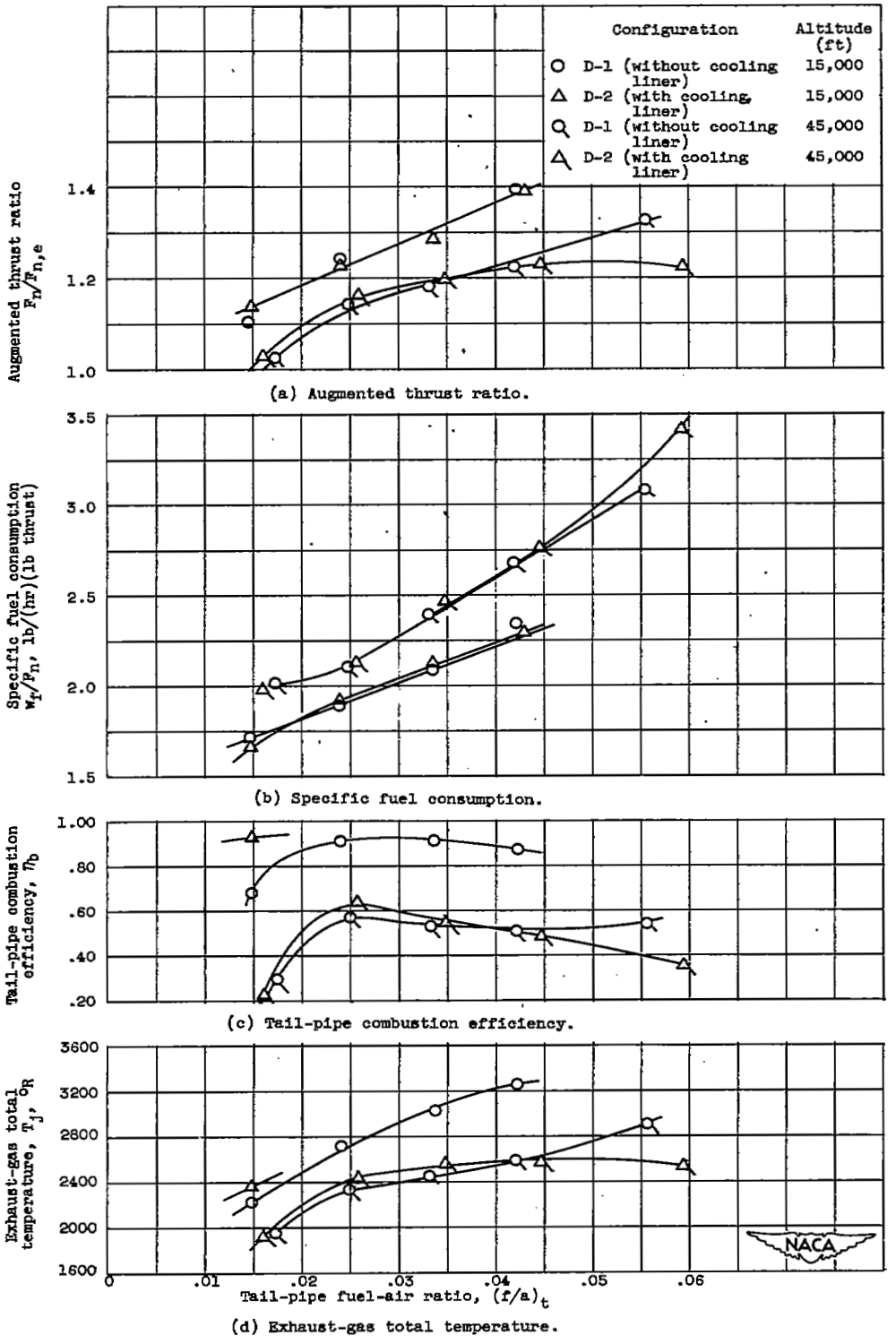

Figure 21. - Effect of cooling liner on afterburner performance. Flight Mach number, 0.21; engine speed, 7900 rpm.

[redacted]